University of Nevada, Reno

Low Temperature Phase Transitions of Gadolinium and Ytterbium Using Resonant Ultrasound Spectroscopy

A dissertation submitted in partial fulfillment of the
requirements for the degree of
Doctor of Philosophy in Physics

by

Gunes Sakallioglu Kaplan

Dr. Katherine R. McCall, Dissertation Advisor

December 2017

THE GRADUATE SCHOOL

We recommend that the dissertation
prepared under our supervision by

GUNES SAKALLIOGLU KAPLAN

entitled

Low Temperature Phase Transitions of Gadolinium and Ytterbium Using Resonant Ultrasound Spectroscopy

be accepted in partial fulfillment of the
requirements for the degree of

DOCTOR OF PHILOSOPHY

Katherine McCall, Ph.D., Advisor

Tim Darling, Ph.D., Committee Member

Aaron Covington, Ph.D., Committee Member

Danesh Chandra, Ph.D., Committee Member

Sean Casey, Ph.D., Graduate School Representative

David W. Zeh, Ph.D., Dean, Graduate School

December, 2017

ABSTRACT

Low temperature phase transitions in the lanthanides gadolinium (Gd) and ytterbium (Yb) were studied using the nondestructive technique of resonant ultrasound spectroscopy (RUS) coupled with a cryogenic system. Previous studies of these materials utilized a pulse-echo method that is not as robust as RUS. The advantages of RUS include the ability to study very small samples and the ability to obtain all elastic properties of the sample from a single frequency spectrum. A laboratory system was developed combining RUS with a cryogenic cooling system capable of exploring the temperature range 13 K 340 K. The complex 4-f electronic structure of elemental Gd and Yb leads to continuous magnetic and first-order structural phase transitions within this temperature range. The results of measurements on Gd are consistent with those previously reported in literature, supporting the validity of RUS measurements on small lanthanide samples at low temperature. Three new phenomena are observed in the Yb measurements: a positive slope in resonance frequency versus temperature, hysteresis around a previously reported transition temperature of 315 K that decreases with temperature cycling, and hysteresis at low temperatures with discrete memory characteristics.

Dedicated to the three men in my life:

To my *father* who seeded the foundations of my knowledge...

To my *husband* whose commitment, support and patience have been endless...

To my *son* whom I really hope that I was able to inspire with the importance and value of education no matter how old one is...

Acknowledgments

The completion of this dissertation has been a long journey. Especially in the last couple of years, though pretty much abandoned, it was never forgotten. Many have questioned whether or not I would finish my dissertation and had doubts in my commitment to it. Not being able to complete it felt like a dark failure which haunted me... Then, I returned to it because I knew I'd complete my PhD. Although it has always been a priority in my life, due to the challenges in life it couldn't always be the number one priority. I have finally finished it and I am proud and delighted that it is finally completed. There are several people without whom this task would have not been completed. Without these people, especially the ones I'm about to mention, I may not have gotten to where I am today with my dissertation.

First and foremost, I am indebted to my thesis advisor, Dr. Katherine McCall, who has made the process of dissertation writing into an extraordinary intellectual experience for me. I deeply appreciate her detailed critical comments on my chapter drafts which sharpened my thinking and enhanced my understanding. Not only has she encouraged me to work harder and more thoughtfully, but also has showed great efforts and commitment towards the editing and completion of this dissertation. What I have learned from her during the writing process also set new standards for my skills in my job. This indeed extended beyond her task as an academic advisor. I'm grateful for her supervision and I owe her the greatest degree of appreciation. Thank you, Dr. McCall.

I'd also like to give a heartfelt, special thanks to Dr. Tim Darling. He was

my mentor since the very beginning, a foundation of information, a patient teacher always available to answer my questions, to help me out with my analysis and with many other things. Even after his retirement, he remained a supporter and provided insight and direction-right up to the end. For all of these, I cannot thank Dr. Darling enough.

Thirdly, I am very grateful for the remaining members of my dissertation committee, Dr. Aaron Covington, Dr. Sean Casey and Dr. Danesh Chandra for their interest in my work, input, and their willingness to be in my committee.

I must also mention my colleagues at the Nevada Department of Education, Dr. Kate Rohrer, Russ Keglovits and Dr. Kevin Marie Laxalt for their constant encouragement, support, and humor.

In addition, these acknowledgements would not be complete if I did not mention the sponsors of this work and myself. Support for this project was generously provided from Nevada Terawatt Facility (NTF) under the U.S. DOE grant no DE-FC52-01NV14050 at UNR. I'd also like to thank to the UNR Grant-in-Aid Benefits Program for financially supporting me in my graduate school enrollments during the last couple of semesters.

This last piece of acknowledgement I have saved for my dear husband Ali Sakallioglu whom I'd like to thank for his love, sacrifices and support that he has showed in every possible way to see the completion of this work. I owe him a lot.

Table of Contents

List of Tables

List of Figures

Chapter 1

Introduction

Scientific research and development during the last fifty years in the areas of condensed matter and materials physics has extended our understanding of materials from single crystals, simple compounds and alloys, to a better understanding of complex systems such as granular materials, polycrystals, superconductors, and magnetic materials. Materials physics, the study of the physical properties and behavior of complex media, has become one of most significant areas of applied physics. A subfield of materials physics is the study of material characteristics and behavior under extreme conditions, including very high and very low temperatures, high pressure, high mechanical stresses, and exposure to high magnetic or electric fields. As technological advances permit researchers to create extreme conditions in a controlled laboratory environment, the consequent studies of materials under extreme conditions fuel further scientific, technological, and engineering advances.

The following dissertation describes a materials physics study of matter under extreme conditions. The elastic behavior of polycrystalline lanthanides gadolinium (Gd) and ytterbium (Yb) was studied as a function of temperature, with a focus on low temperatures (77 K - 300 K). The result is a systematic study of the phase transitions in these lanthanides over the relevant temperature range, and how these phase transitions are influenced by sample microstructure, initial phase, and temperature. Phase transitions are not only technologically important but also enjoyably challenging to study because they are influenced by many factors, including crystal structure and symmetry, polycrystal bonding, and thermodynamic response. The primary experimental method used to track the elastic behavior and thus phase transitions in Gd and Yb was resonant ultrasound spectroscopy (RUS).

From the outset, our sample microstructure was expected to have an influence on the measured elastic behavior. Microstructure refers to the structural organization of the material on the molecular, grain, and multigrain scale. Important microstructural characteristics include crystal structure, grain size, crystal and grain orientation, and crystal and grain composition. Variations in microstructure across samples can effect macroscopic physical properties such as strength, toughness, ductility, hardness, and corrosion resistance. The physical properties of all technologically interesting materials are strongly dependent upon their microstructure, and thus, control of sample microstructure is highly desirable. The most efficient way of obtaining a desired microstructure is via accurate control of phase transformations in the material.

When a material or portion of a material has homogeneous composition and uniform physical properties, it is said to be in a particular phase. Phases can coexist in a material in physically distinct portions of the material. The phase, or phases, of a material determine important macroscopic physical properties such as elasticity. In this particular work, the elastic constants of a material (the second derivatives of the free energy with respect to strain) are used as sensitive indicators of phase transitions as temperature is varied. Elastic constants reflect fundamental thermodynamic properties of the crystal lattice in solids. From the point of view of lattice stability, the temperature dependence of the elastic constants is more important than their absolute values.

The experimental chamber designed for this research supports measurements over a broad temperature range, including temperatures far below those generally experienced on the Earth's surface. At low temperatures, material properties become less entangled with each other. In a sense, the material behavior becomes simpler such that individual properties can be probed with minimal interference. Low temperatures are particularly useful for probing crystal lattice vibrations, superconductivity, and magnetism. "Low temperature physics" is an area of research devoted to measuring and understanding physical properties in the temperature range 0 - 4 K. In this research, the desired environment was not quite so extreme. Most of the measurements were made using liquid nitrogen as a coolant, such that the lowest temperature obtained was 77 K, still far below 273 K, the freezing temperature of water.

There has been a growing interest in the ability to measure elastic properties of materials using nondestructive methods. Although the definition of elasticity - the ability of a material to change shape in response to a force and then regain its initial shape is the same for all materials, measurement techniques vary widely. The resonant ultrasound spectroscopy (RUS) technique was chosen as the experimental method for this work. Natural (resonant) frequencies of free elastic vibrations of a small specimen are measured for a number of the sample's normal modes. The elastic constants of the sample are then inferred from the resonant frequencies. This is an inverse process, i.e., if the elastic constants of a sample are known, the resonant frequencies can be calculated directly. RUS analysis attempts to do the inverse and use known frequencies to calculate unknown elastic constants. Sophisticated nonlinear inversion procedures have been developed that are quite successful and easy to use. Thus RUS has become a fairly standard and powerful technique for monitoring elastic properties of materials. The temperature dependence of elastic constants can be very conveniently measured by the RUS method because a complete set of all constants is obtained from a single measurement.

In a nutshell, the measurements described in this dissertation were intended to discover and confirm low-temperature phase transitions in the lanthanides Gd and Yb. Lanthanides are elements of rapidly growing importance. The interesting properties of the lanthanide metals and lanthanide-based materials arise from the open 4f electron shell that remains almost atomic like in the

condensed phase. The 4f electronic structure of Gd and Yb influences the temperatures and pressures at which magnetic and electronic phase transitions and first order structural transitions occur. The following paragraphs give a quick description of Gd and Yb and their applications. For more detail, see references [1], [2], and [3].

Gadolinium has a hexagonal close-packed (hcp) structure with a constant c/a ratio of 1.59 at atmospheric pressure and temperatures below 1500 K. It exhibits a complex magnetic spin structure with strong dependence on temperature, resulting from its localized 4f electron. As temperature is uniformly changed, Gd exhibits magnetic phase transitions at 100 K, 224 K, and between 295-310 K. In the electronics industry, oxides of gadolinium are used in the production of various types of ferrites. Gadolinium yttrium garnets have microwave applications. Compounds of gadolinium have been used for making green phosphors in color TV tubes and in the production of compact discs and computer memory hardware. Metallurgically, the addition of a very small amount of gadolinium (as small as 1%) improves the resistance of various metals and related alloys to high temperatures and oxidation.

In the nuclear field, Gd is one of the best thermal neutron absorbers and is therefore used in shielding of nuclear reactors. In some reactors Gd is used as a secondary emergency shutdown measure or to detect radiation leaks in power plants. Gd is used in nuclear marine propulsion systems as a burnable poison. Burnable poisons are materials that are obtained by converting high neutron absorption cross section materials into relatively low absorption cross section

materials. They are loaded into reactor cores to control large amounts of excess fuel reactivity. In the military, gadolinium compounds are used in radar systems, phase shifters, and in the tuners and filters used in the guidance of air defense missile systems such as the PATRIOT.

Although gadolinium has no known native biological role, its compounds are widely used in biomedical research tools. Gd compounds are used to improve the visibility of internal body structures in magnetic resonance imaging (MRI). and to convert X-rays released from a source into light. In nuclear medicine, Gd single crystal compounds are the scintillators in positron emission tomography (PET). Finally, due to its high neutron capture cross section, Gd is widely used in neutron radiography as a neutron shield.

Ytterbium is one of the two rare earth metals which have a completely occupied 4f electron shell ($4f^{14}$). It has two electrons per atom in the conduction band. Among the divalent elements, Yb exhibits the most unusual physical properties. Its lattice dynamics have not been understood very well and it exists in three different crystal structures: body-centered cubic (bcc), face-centered cubic (fcc), and hexagonal close-packed (hcp). At atmospheric pressure and temperatures below 300 K, the crystal structure is hcp; however, for temperatures between room temperature and 1000 K, the crystal structure is fcc, and the transition displays substantial hysteresis around room temperature.

In the medical field, one of ytterbium's seven isotopes is used as a radiation source for portable x-ray machines when electricity is not available.

Another isotope of ytterbium is used in the medical treatment of prostate cancer. Metallurgically, since ytterbium is an alloying agent, a small amount of Yb is used to improve the grain refinement, strength and other mechanical properties of stainless steel. Similarly, it is used in the glass and ceramics industry to add strength to the material. In the optical and electronics industry, low concentrations of ytterbium are often used as a doping material for high power and high wavelength tunable solid state lasers. In telecommunications, Yb is added to optical fiber cables to create amplifiers.

Ytterbium also has uses in the solar cell industry, as it can convert infrared energy into electricity in solar cells. Some compounds of ytterbium absorb and emit radiation in the near infra-red and this makes them useful probes for examining biological tissues. An interesting use of elemental ytterbium is in super accurate atomic clocks. One of its isotopes has the potential to keep time extremely accurately, losing a second every 100 million years. Ytterbium metal increases its electrical resistivity when subjected to high stresses. This property is used in stress gauges to monitor ground deformations from earthquakes and explosions.

This dissertation is divided into six chapters. Chapter 2 provides some background information and a literature review evaluating previously published work. In Chapter 3, the theoretical and general principles of the primary experimental method are described, a short summary of the RUS method is given, and some representative resonance measurements at room and low temperatures are displayed. More about the experimental design and techniques is included in

Chapter 4. The experimental results are presented in Chapter 5 under sub categories for each of the samples studied. Experiments testing the stability and performance of our cryogenic system are also described in Chapter 5. Chapter 6 contains conclusions.

Chapter 2

Background and Literature Review

2.1 Some property comparisons

Gadolinium (Gd) and ytterbium (Yb) and are both rare-earth metals of the lanthanide series with a hexagonal close-packed (hcp) crystal structure at atmospheric pressure and low temperatures (less than 300 K). The hcp structure is illustrated in Figure 2.1. Although similar in this narrow range of temperature and pressure, their phase diagrams are markedly different from each other over a broader range, as illustrated in Figure 2.2. These differences may be attributed in part to the atomic electron configurations.

The lanthanides constitute lanthanum (electron configuration [Xe]$5d^1 6s^2$) and the next 14 elements, and are distinguished by having electrons filling the $4f$ electron shell, which can hold 14 electrons. Foe example, gadolinium is the seventh element after lanthanum and has an electron configuration [Xe]$4f^7 5d^1 6s^2$. The half-filled $4f$ shell is very stable and the $4f$ electrons are deeply buried in the atom,

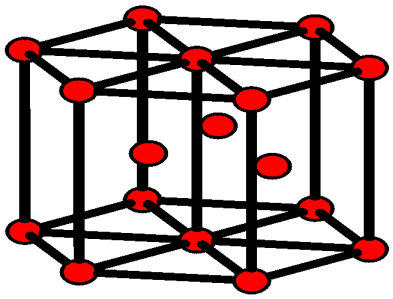

Figure 2.1: Hexagonal close-packed structure [4].

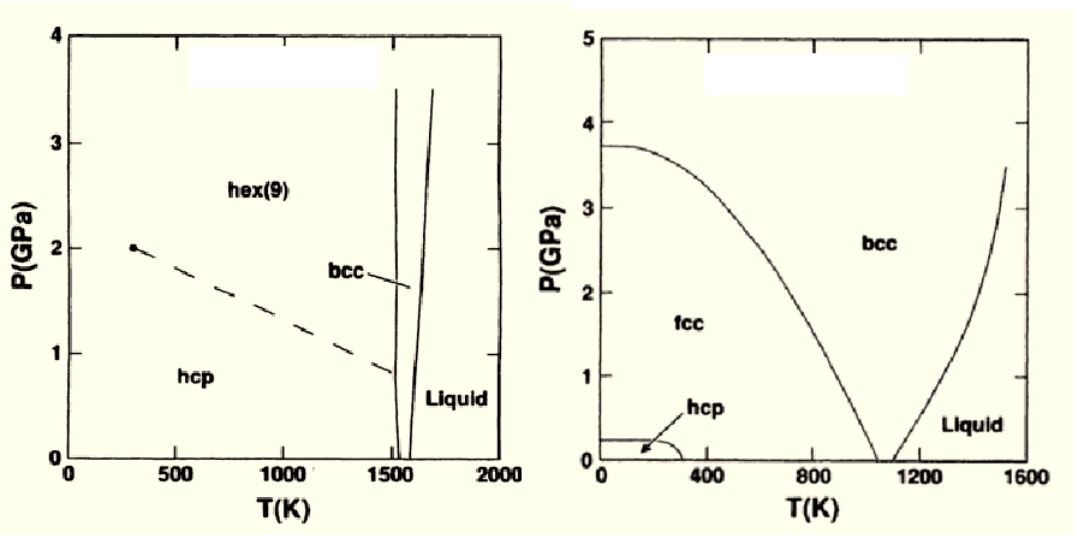

Figure 2.2: Phase diagrams of gadolinium (left) and ytterbium (right) [5].

i.e., they are shielded by the filled $5s^2$ and $5p^6$ electron shells characteristic of the noble gas xenon. Thus only the three $5d^1 6s^2$ electrons are valance electrons and participate in bonding; gadolinium is considered trivalent.

Ytterbium is the thirteenth element after lanthanum and generally fills its $4f$ electron shell, rather than have a single $5d$ electron. Thus its equilibrium electron configuration is $[\mathrm{Xe}]4f^{14}6s^2$. In general, ytterbium is considered divalent and has two bonding electrons, however, the energy difference between the $4f$ and $5d$ levels is small enough that in certain environments, Yb will be trivalent. While the mechanical properties of gadolinium follow a general trend in the lanthanide series, ytterbium tends to be an outlier along with europium.

Gadolinium and ytterbium have been studied extensively as a function of pressure and for a broad range of temperatures. In the following sections, only literature specific to elastic or structural behavior at atmospheric pressure and room temperature or below is reviewed.

2.2 Gadolinium

According to the structural phase diagram of gadolinium (Figure 2.2), the polycrystalline metal is hcp throughout the low pressure, low temperature regime. Thus, measurements of the elastic behavior of Gd as a function of temperature should not produce any behavior suggesting first-order structural phase changes. However, magnetic ordering can change without a structural change. Since elastic constants and magnetic susceptibility are both second derivatives of the internal

energy of a system, the elastic behavior of a system can indicate changes in magnetic ordering.

M. Rosen [6] used this reasoning to motivate his measurements of the elastic moduli of polycrystalline gadolinium. Rosen measured the longitudinal and transverse acoustic velocities (v_L and v_T respectively) of high purity polycrystalline Gd by an ultrasonic pulse technique at a frequency of 10 MHz between 4.2 and 300 K. Using standard relationships, he determined the variation with temperature of the Young modulus (E), shear modulus (G), Debye temperature (Θ_D), and adiabatic compressibility (K_S). His results are shown in Figures 2.3 and 2.4, where

$$G = \rho v_T^2, \quad E = 2\rho v_T^2(1+\nu), \quad K_S = \frac{3(1-2\nu)}{2\rho v_T^2(1+\nu)}, \tag{2.1}$$

and

$$\Theta_D = \frac{h}{k_B}\left[\frac{9N\rho}{4\pi M\left(\frac{2}{v_T^3}+\frac{1}{v_L^3}\right)}\right]^{1/3}, \tag{2.2}$$

where

$$\nu = \frac{2-\left(\frac{v_L}{v_T}\right)^2}{2\left[1-\left(\frac{v_L}{v_T}\right)^2\right]} \tag{2.3}$$

is the Poisson ratio, ρ is the measured sample density, h is Planck's constant, k_B is Boltzmann's constant, N is Avogadro's number, and M is atomic weight.

From Figures 2.3 and 2.4, it is immediately obvious that gadolinium has interesting magnetic behavior. In fact, gadolinium is one of five ferromagnetic elements, along with iron, cobalt, nickel, and dysprosium. A ferromagnet is a material that behaves as a paramagnet above a certain temperature (T_C, the Curie

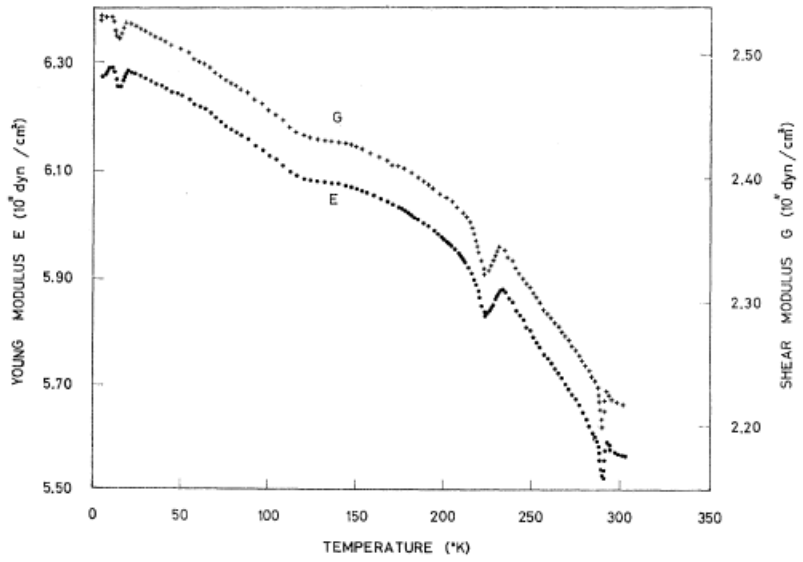

Figure 2.3: Temperature variation of Young's and shear moduli of polycrystalline gadolinium [6].

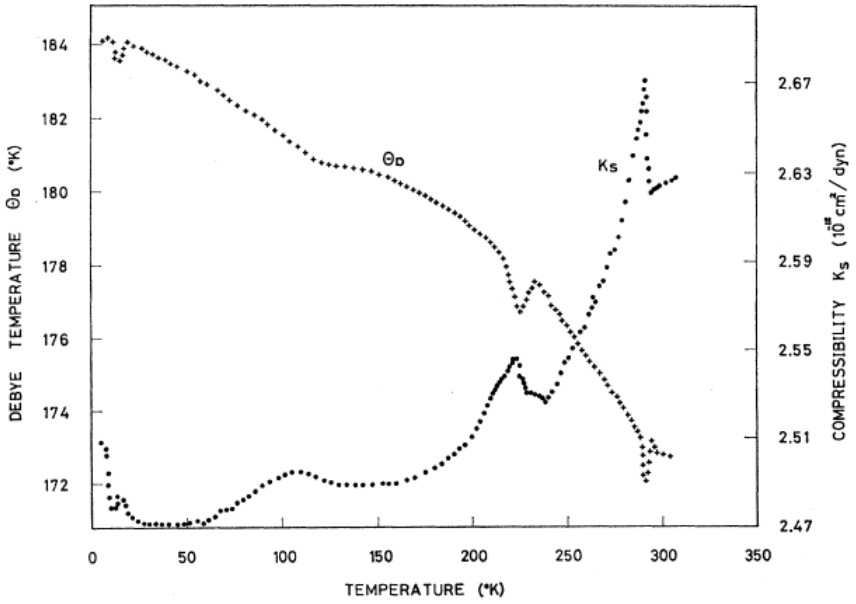

Figure 2.4: Temperature variation of Debye temperature and compressibility of gadolinium [6].

temperature) and has a spontaneous magnetic moment, even in zero magnetic field, below T_C. Gadolinium has a fairly low Curie temperature where it undergoes a second order paramagnetic - ferromagnetic phase transition with a critical exponent $\gamma \approx 1.3$ [7]. The critical exponent γ describes how the susceptibility χ changes very close to T_C:

$$\chi = \frac{1}{V}\frac{\partial M}{\partial H} \sim \left|\frac{T - T_C}{T_C}\right|^{-\gamma}, \tag{2.4}$$

where V is volume, M is the magnetization, and H is the external magnetic field. The accepted value of T_C is 292.5 K, and published measurements are generally in the range 292 - 294 K [8, 9, 10].

While Rosen's data clearly expose the paramagnetic - ferromagnetic transition at 292 K, they also expose a second possible transition at 224 K. Rosen attributed the discontinuity in elastic behavior to a dramatic change in the easy direction of the spontaneous magnetization that was measured by Graham [11]. Below the Curie temperature, many ferromagnets develop their spontaneous magnetization preferentially in a particular crystallographic direction [12]. This is called the easy axis of magnetization. The easy direction can have strong temperature dependence, as is the case for gadolinium. Just below T_C, gadolinium develops magnetization preferentially in the c direction (the vertical direction in Figure 2.1). This remains true for the 50 degrees below T_C. At approximately 224 K, the easy axis of magnetization begins to tilt away from the c direction to form a cone angle with the c axis. In more recent publications, this transition point is called the spin reorientation temperature, T_{SR}, and measured values are in the

range 220 - 230 K [8, 9, 10]. Graham measured a dramatic shift of the axis of magnetization moving all the way to the basal plane before returning to a cone angle of 30 degrees at very low temperatures. Other measurements compiled by McEwen [13] and shown in Figure 2.5 show similar, but less dramatic changes in the easy magnetization direction with the same low-temperature asymptote in the cone angle.

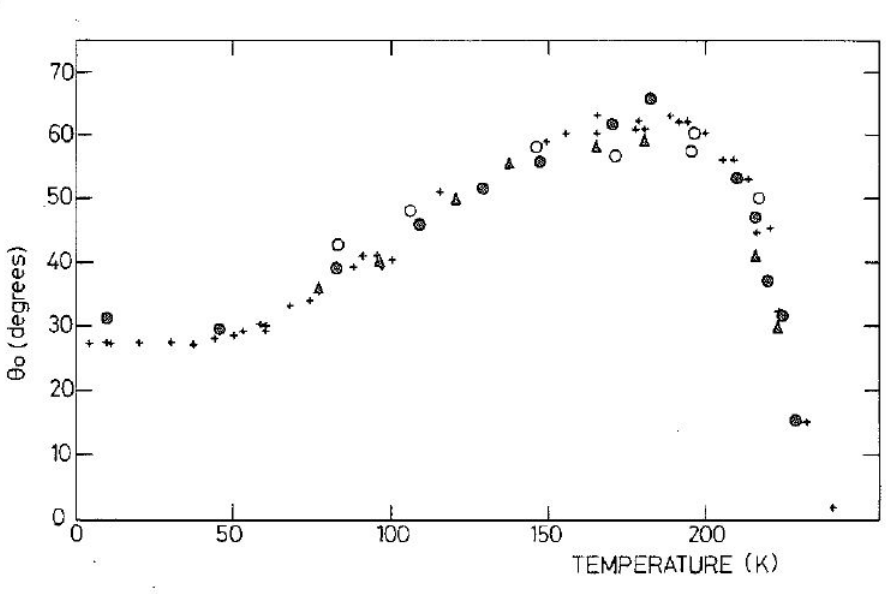

Figure 2.5: Temperature dependence of the easy magnetization direction for gadolinium [13]. The angle is measured with respect to the c-axis in the fcc structure. Open and closed circles are from Cable and Wollan [14]. Crosses and triangles are from Corner and Tanner [15].

There are two other temperatures of interest in Rosen's data at approximately 115 K and 15 K. Rosen speculated that the easy cone of magnetization changes its angle with respect to the c axis at 115 K and that the transport properties change at 15 K. However, these property changes and their characteristic temperatures have not been definitively confirmed by other researchers. The possible transition at 115 K is within the temperature range of the

Reference	T(K)	E(GPa)	G(GPa)	B(GPa)
Gust and Royce [17]	298	56.1	22.3	38.5
Smith et. al. [16]	298	56.2	22.3	38.9
Rosen [6]	300	55.6	22.2	38.1
Rosen [6]	0	62.7	25.2	39.9

Table 2.1: Measured elastic moduli of polycrystalline gadolinium, primarily at room temperature. T stands for Temperature, E for Young's modulus, G for shear modulus and B for bulk modulus.

experimental system described here and for clarity in the discussion, it is labeled T_R.

Two other research groups [16, 17] used the ultrasonic pulse technique to measure the Young modulus, shear modulus, and compressibility of polycrystalline gadolinium at room temperature. Table 2.1 shows a compilation of these measurements. Measurements of Young's modulus as a function of temperature have been made on single crystal gadolinium [8, 9, 10], and show that the magnitudes change with crystal orientation, but the trends and transitions are similar to those originally measured by Rosen (Figures 2.3 and 2.4).

2.3 Ytterbium

The most cited study on the temperature dependence of the elastic properties of polycrystalline ytterbium was completed by M. Rosen in 1971 [18]. Using the same experimental technique described for Gd in Section 2.2, he obtained the Young and shear moduli shown in Figure 2.6, and the adiabatic compressibility and Debye temperature shown in Figure 2.7.

The moduli and Debye temperature in Figs. 2.6 and 2.7 vary smoothly,

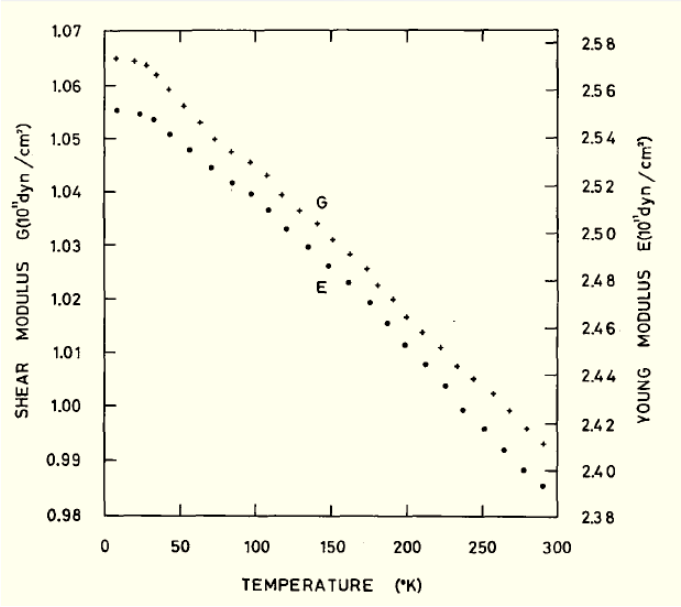

Figure 2.6: Temperature variation of Young's (E) and shear (G) moduli of ytterbium [18].

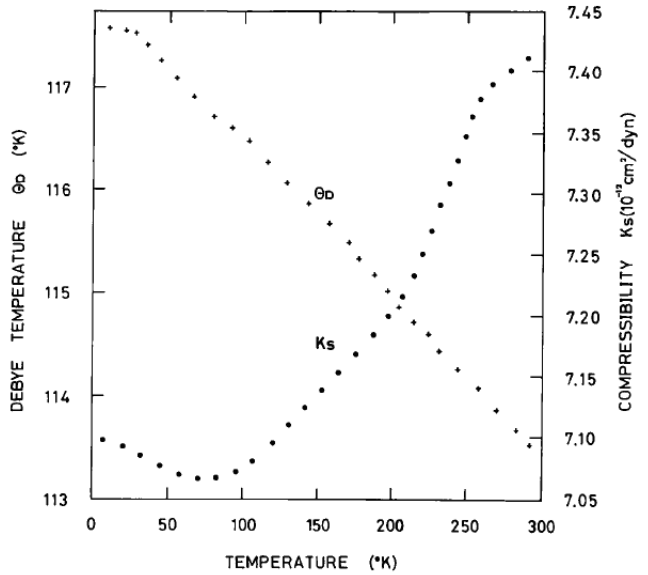

Figure 2.7: Temperature variation of the adiabatic compressibility (K_S) and the Debye temperature (Θ_D) of polycrystalline ytterbium [18].

Reference	T(K)	E(GPa)	G(GPa)	B(GPa)
Gust and Royce [17]	298	18.8	7.3	15.0
Smith et. al. [16]	298	17.8	7.0	13.8
Rosen [18]	300	23.9	9.9	13.5
Rosen [18]	0	25.5	10.7	14.1

Table 2.2: Measured elastic moduli of polycrystalline ytterbium, primarily at room temperature. T stands for Temperature, E for Young's modulus, G for shear modulus and B for bulk modulus.

decreasing as temperature increases and leveling to a zero degree asymptote, as expected for a stable material with no obvious phase transitions. The only indication of unusual behavior is in the adiabatic compressibility, which has a minimum around 75 K. The low temperature asymptote is not the minimum value of K_S, as expected. Rosen offered no explanation of the unexpected change in slope. Table 2.2 is the analog of Table 2.1 for ytterbium. Note that the agreement between room temperature measurements is much higher for gadolinium than for ytterbium.

At the time of his measurements, Rosen and others assumed that ytterbium metal has an equilibrium fcc structure at atmospheric pressure and temperatures below 300 K. However, the early 1970s were a time of great interest in the physical properties of the lanthanides, and several other studies of ytterbium were taking place simultaneously. Measurements of the susceptibility [19], resistivity [20] and de Haas-van Alphen effect [21], among others, established that pure and unstrained samples of polycrystalline ytterbium metal have an hcp structure at low pressures and for temperatures below approximately room temperature, as illustrated in Figure 2.2. Young [5] places the transition temperature at 310 K.

In addition to a martensitic structural change in the low pressure and

temperature region of the phase diagram, Yb undergoes a magnetic phase change. The fcc structure is paramagnetic (the magnetic moment is parallel to the applied field), while the hcp structure is diamagnetic (the magnetic moment opposes the applied field) [19, 22]. The phase transition is highly hysteretic over a temperature range that is dependent on sample purity, internal stress, and pressure. Alderson and Hurd [22], for example, found that in an evacuated chamber the transition, measured through resistivity and Hall coefficient, occurs over the range 150 - 250 K upon cooling and over 320 - 370 K upon heating, as illustrated in Figure 2.8. Bucher et al. [19] saw similar hysteresis in the magnetic susceptibility with a repeatably sharp transition from hcp to fcc upon warming at 315 K, as shown in Figure 2.9.

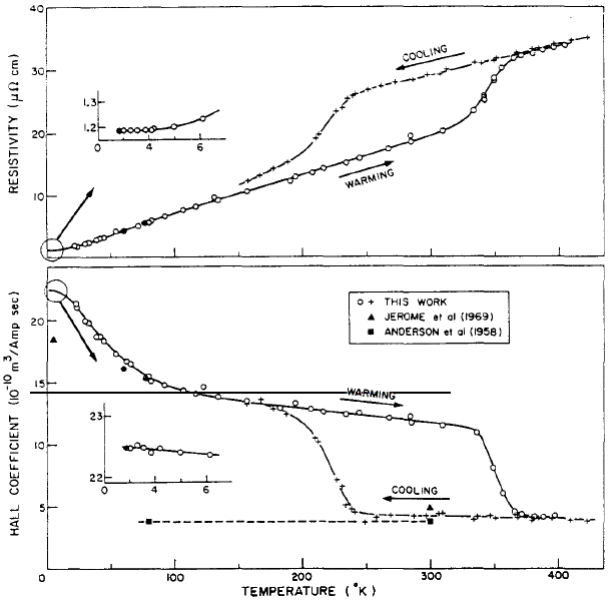

Figure 2.8: Hysteretic phase transition in ytterbium [22].

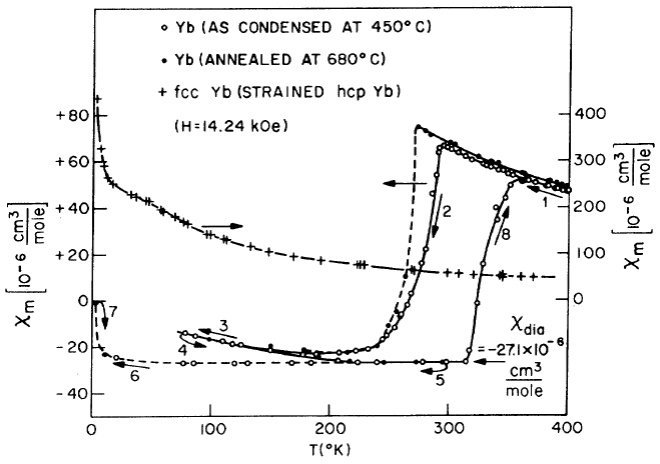

Figure 2.9: Temperature dependence of magnetic susceptibility of ytterbium [19].

2.4 Measurement expectations

Rosen and others have demonstrated that measurements of the elastic properties of ytterbium and gadolinium are sensitive to both structural and magnetic property changes as a function of temperature. The resonance measurements described in the next chapters of this dissertation have the potential to be more sensitive and more accurate than the traditional pulse-echo method of measuring elastic properties. Measurements at atmospheric pressure and for 77 - 300 K may then be expected to yield a large amount of hysteresis in ytterbium, caused by structural changes, and two to three magnetic property changes in gadolinium.

Chapter 3

Resonant Ultrasound Spectroscopy: Theory and Measurement Basics

The temperature dependence of the natural frequencies of vibration of a solid object can be very conveniently measured by resonant ultrasound spectroscopy (RUS), a nondestructive technique for investigation of elastic properties of solids. The advantages of RUS over techniques such as pulse echo include the ability to make measurements on very small samples and the ability to obtain all of the elastic properties of the sample from a single frequency spectrum.

Comprehensive descriptions of the development of RUS are given in at least one book and two reviews [24, 25, 26]. A brief sketch is given here. The first application of RUS in materials science was a 1964 measurement by Frazer and

LeCraw [27] using a single transducer set up to measure the resonant frequencies of a sphere. Later, the geophysicists Soga and Anderson [28] improved the experimental configuration by adding a second transducer, providing both more measurement flexibility and a way to hold the sample in place. This configuration, where the sample is held between two transducers is the most commonly used configuration today. In 1971, Demarest [29], a student of Anderson, made a great breakthrough by developing the computational analysis technique that makes it possible to apply RUS to cubic symmetry. And in 1976, Ohno [30] provided the analysis solution for parallelepiped shaped samples with various symmetries. RUS took its present form in 1988 when Migliori extended the limits of the RUS technique by improving the experimental hardware and low-level electronic measurements, and Visscher developed some highly efficient computer algorithms to improve the analysis [31]. Later, Maynard developed a method to apply RUS to very small sample sizes [24]. The term resonant ultrasound spectroscopy was introduced to the physics community by Migliori to promote the technique. This term is used to describe all techniques of elastic modulus determination that use acoustic resonant frequencies.

The purpose of this work is to detect phase transitions by investigating changes in the measured resonance spectrum and calculated elastic constants of a sample as a function of temperature. The measured resonance spectrum of a sample, together with its geometry, density, and an initial estimate of the elastic constants are the ingredients used to determine the elastic constants of the sample. Elastic constants are related to the atomic bonding and thermal properties of a

solid material. They are directly linked to many fundamental physical phenomena such as the equation of state, lattice dynamics, phonon spectra, thermal expansion, Debye temperature, and Grüneisen parameters characteristic of the sample material.

3.1 Linear Elasticity Theory and Elastic Constants

Resonant ultrasound spectroscopy works because the resonances of a material are directly connected to the elastic properties of the material through linear elasticity theory. The following is a brief description of linear elasticity theory and its connection to the analysis used for RUS data [25].

Solid materials are deformed when forces are applied to them. In other words, solid materials become strained when they are subjected to a stress. When the deformation occurs, every point in the body may be displaced. If the coordinates of a point before deformation are (x_1, x_2, x_3), then the displacement of that point can be written as $u_i(x_k)$ where $i, k = 1, 2, 3$ representing the three Cartesian coordinates. The deformation in an element of length in the material is given by the strain tensor (for small deformations)

$$\varepsilon_{kl} = \left[\frac{\partial u_k}{\partial x_l} + \frac{\partial u_l}{\partial x_k}\right]. \tag{3.1}$$

The forces causing this deformation can be written in terms of the stress tensor σ_{ij} where i denotes which component of the force is acting and j denotes the

axis along which the normal lies. In principle, elastic constants can be computed from the stress-strain relationship, or generalized Hookes law, in three dimensions:

$$\sigma_{ij} = \sum_{k=1}^{3} \sum_{l=1}^{3} c_{ijkl} \varepsilon_{kl}, \tag{3.2}$$

where c_{ijkl} is a rank four tensor of elastic constants that links two second-rank tensors. Due to symmetry, this rank four tensor can be written using two subscripts, representing the first two and last two subscripts of the initial tensor, as illustrated in Table 3.1. The resulting c_{ij} matrix has 36 components that are symmetric with respect to reversed indices, further reducing the number of independent elastic constants to 21. Crystal symmetry reduces the number of independent elastic constants further. In an isotropic system, for example, when the properties of a material are the same in all directions, only two constants c_{11} and c_{44} are needed to fully describe the elastic properties. These elastic constants are related to the familiar shear modulus μ and bulk modulus B by the relations $c_{44} = \mu$ and $c_{11} = B + 4\mu/3$.

Tensor	11	22	33	23,32	31,13	12,21
Matrix	1	2	3	4	5	6

Table 3.1: Reduction of subscripts in c_{ijkl} from four to two. Two subscripts (first two and last two) in the tensor are replaced by the corresponding matrix subscript.

The materials used in this work are polycrystalline and assumed to be isotropic, i.e., the wavelength of resonances excited in the samples is large enough to average over grain and crystal orientation, yielding an effectively isotropic material.

This is by design, since RUS analysis packages are most fully developed and dependable for isotropic solids. The derivation of elastic constants from measured resonance frequencies is an indirect process. That is, sample geometry, density, and elastic constants can be used to directly calculate resonance frequencies (as described in Section 3.2), but the inverse is not a direct linear calculation. RUS analysis proceeds by estimating elastic constants, directly calculating the expected resonance frequencies, comparing the calculated frequencies to the measured resonance frequencies, and then modifying the estimated elastic constants to minimize the difference between calculated and measured frequencies. The theory behind the forward calculation of frequencies from physical constants is sketched in Section 3.2. The concept behind the inverse minimization of frequency differences is described in Section 3.3.

3.2 Calculating the Resonance Frequencies of a Body: The Forward Calculation

Lagrangian dynamics and Hamiltons variational principle are the relevant theoretical tools used to connect elastic constants and resonances of a body. The principles involved are illustrated here with a one-dimensional example: a vibrating string of length l, uniform mass density σ, and under uniform tension τ. The

general form of the Lagrangian L [32] is

$$L = \int_0^l \left[\frac{1}{2}\sigma \left(\frac{\partial u}{\partial t} \right)^2 - \frac{1}{2}\tau \left(\frac{\partial u}{\partial x} \right)^2 \right] dx, \tag{3.3}$$

where $u(x,t)$ is the transverse displacement of the string, the first term is the kinetic energy density and the second term is the potential energy density.

Hamilton's principle states that for fixed endpoints in time,

$$\delta \int_{t_1}^{t_2} L dt = 0. \tag{3.4}$$

Varying L by varying u arbitrarily in the Lagrangian of Eq. (3.3) ($L \to L + \delta L$ when $u \to u + \delta u$), the variation of the Lagrangian integrated in time is

$$\int_{t_1}^{t_2} \delta L dt = \int_0^l \left(\sigma \frac{\partial u}{\partial t} \delta u \Big|_{t_1}^{t_2} \right) dx - \int_{t_1}^{t_2} \left(\tau \frac{\partial u}{\partial x} \delta u \Big|_0^l \right) dt + \int_{t_1}^{t_2} \int_0^l \left(\tau \frac{\partial^2 u}{\partial x^2} - \sigma \frac{\partial^2 u}{\partial t^2} \right) \delta u dx dt, \tag{3.5}$$

where only terms first-order in δu have been retained, and terms have been integrated by parts when possible.

The first term in Eq. (3.5) vanishes because Hamilton's principle requires fixed endpoints in time, i.e., $\delta u(x, t_1) = \delta u(x, t_2) = 0$. The last term vanishes if the string obeys the usual one-dimensional string equation,

$$\tau \frac{\partial^2 u}{\partial x^2} = \sigma \frac{\partial^2 u}{\partial t^2}. \tag{3.6}$$

The second term vanishes for a variety of boundary conditions: both ends fixed

($\delta u(0,t) = \delta u(l,t) = 0$), both ends free ($\partial u/\partial x|_0 = \partial u/\partial x|_l = 0$), or a combination of the two (one end fixed, one end free).

RUS analysis assumes free boundaries on the sample and looks for harmonic solutions to the equation of motion (e.g., Eq. (3.6)) in the form of a sum of polynomials [31]. In one dimension, the displacement can be written

$$u(x,t) = \sum_n a_n x^n e^{i\omega t}. \tag{3.7}$$

Substituting Eq. (3.7) into the Lagrangian and varying the Lagrangian by varying the polynomial term amplitudes a_n ($L \to L + \delta L$ when $a_n \to a_n + \delta a_n$), the eigenvalue equation satisfying Hamilton's principle for arbitrary δa_n is

$$(\omega^2 \mathbf{E} - \mathbf{\Gamma})\mathbf{a} = 0, \tag{3.8}$$

where

$$E_{nm} = \frac{\sigma l^{n+m+1}}{n+m+1}, \tag{3.9}$$

and

$$\Gamma_{nm} = nm\tau \frac{l^{n+m-1}}{n+m-1}. \tag{3.10}$$

The eigenvalues of Eq. (3.8) are the resonance frequencies of the body, $\omega_n = 2\pi f_n$, and are found by setting the determinant $|\omega^2 \mathbf{E} - \mathbf{\Gamma}| = 0$. For each eigenvalue ω_n, there is a corresponding eigenvector $\mathbf{a}_n$ that solves Eq. (3.8).

For a (real) three-dimensional sample, the polynomial sum in Eq. (3.7) is

three-dimensional,

$$u(x, y, z, t) = \sum_{l,m,n} a_{l,m,n} x^l y^m z^n e^{i\omega t}. \tag{3.11}$$

and the size of the tensors involved increases dramatically, although the form of the problem remains the same. $\mathbf{E}$ and $\mathbf{\Gamma}$ are the result of volume integrals and can be written as rank-6 tensors, or reduced to symmetric matrices for computational ease. $\mathbf{E}$ is also positive definite. For computational expediency, the sums over polynomial exponents are truncated at a carefully chosen $N \geq l + m + n$. The resulting frequency calculations have been shown to be remarkably accurate when a sample's geometry, density, and elastic constants are known [31].

3.3 Inferring Elastic Constants from Resonance Frequencies: The Inverse Calculation

In Section 3.2, the knowns are the geometry, density, and elastic constants; a linear elasticity theory calculation results in the resonance frequencies. The RUS technique requires knowledge of the geometry and density, and the ability to measure resonance frequencies under free boundary conditions; the elastic constants are to be determined. The numerical solution to this inverse problem begins with a reasonable estimate of elastic constants. A forward calculation of frequencies as described in Section 3.2 is performed. The difference between calculated and measured frequencies is quantified, and this difference is minimized by modifying the elastic constants. The process is iterative and depends somewhat on the choice

of algorithm.

The analysis software code for this research uses the Levenberg-Marquardt algorithm to least-squares fit the data [33]. The following is a description of the Levenberg-Marquardt algorithm, based on that given in "Numerical Recipes" [34]. The idea is to minimize the difference between calculated and measured resonance frequencies by defining and minimizing χ^2, where

$$\chi^2 \equiv \sum_{i=1}^{N} \frac{1}{g_i^2}(f_i - g_i)^2, \tag{3.12}$$

f_i is the i-th calculated frequency and g_i is the i-th measured frequency. For the 1-D example problem, the variable is τ; in a 3-D isotropic case, the variables would be c_{11} and c_{44} (and also include dimensions). In the following, the principles of the χ^2 minimization are illustrated in one dimension.

As mentioned previously, we begin with a reasonable estimate of the elastic constant, in this case τ_0. Taylor expanding χ^2 to second order,

$$\chi^2(\tau) \simeq \chi^2(\tau_0) + (\tau - \tau_0) \left.\frac{\partial \chi^2}{\partial \tau}\right|_{\tau_0} + \frac{1}{2}(\tau - \tau_0)^2 \left.\frac{\partial^2 \chi^2}{\partial \tau^2}\right|_{\tau_0}. \tag{3.13}$$

If χ^2 is a minimum at τ, the derivative of Eq. (3.13) can be set to zero, i.e.,

$$\frac{\partial \chi^2}{\partial \tau} = \left.\frac{\partial \chi^2}{\partial \tau}\right|_{\tau_0} + (\tau - \tau_0) \left.\frac{\partial^2 \chi^2}{\partial \tau^2}\right|_{\tau_0} = 0. \tag{3.14}$$

Solving for $\delta\tau = \tau - \tau_0$, we find

$$\delta\tau = -\frac{\partial\chi^2/\partial\tau|_{\tau_0}}{\partial^2\chi^2/\partial\tau^2|_{\tau_0}} \tag{3.15}$$

In principal, $\delta\tau$ can be calculated directly and added to τ_0 giving a 'better' reasonable estimate of the elastic constant, $\tau_0' = \tau_0 + \delta\tau$. We expect $\chi^2(\tau_0') \leq \chi^2(\tau_0)$ and that the calculation of $\delta\tau$ could be repeated to continue to minimize χ^2 until the fractional difference in subsequent calculations is less than 10^{-3} or any other reasonable choice. In practice, this minimization scheme easily causes χ^2 to blow up rather than decrease. Marquardt's idea was to add a controlling parameter λ in the denominator of Eq. (3.15), such that

$$\delta\tau = -\frac{\partial\chi^2/\partial\tau|_{\tau_0}}{(1+\lambda)\partial^2\chi^2/\partial\tau^2|_{\tau_0}}. \tag{3.16}$$

In the Levenberg-Marquardt algorithm, the iterative procedure begins with a $\lambda \approx 10^{-3}$. If after an iteration, $\chi^2(\tau_0 + \delta\tau) \geq \chi^2(\tau_0)$, then λ is increased by a factor of 10 for the next iteration. If $\chi^2(\tau_0 + \delta\tau) < \chi^2(\tau_0)$, λ is decreased by a factor of 10. The iterative process repeats until the fractional difference in subsequent calculations of χ^2 is less than 10^3 (and χ^2 is decreasing).

A numerical calculation of $\delta\tau$ requires a numerical procedure for finding the first and second partial derivatives of χ^2 with respect to τ. Formally, these are given by

$$\frac{\partial\chi^2}{\partial\tau} = 2\sum_i \frac{1}{g_i^2}(f_i - g_i)\frac{\partial f_i}{\partial\tau}, \tag{3.17}$$

and

$$\frac{\partial^2 \chi^2}{\partial \tau^2} \approx 2 \sum_i \frac{1}{g_i^2} \left(\frac{\partial f_i}{\partial \tau} \right)^2, \tag{3.18}$$

where the additional term in Eq. (3.18) is routinely dropped to save computational time and because it is expected to be very small in comparison to the remaining term [25]. The derivative of calculated frequencies comes from the solutions to the eigenvalue problem derived in the previous section. Given

$$\omega_i^2 \mathbf{E} \mathbf{a}_i = \mathbf{\Gamma} \mathbf{a}_i, \tag{3.19}$$

differentiation with respect to τ produces

$$2\omega_i \frac{\partial \omega_i}{\partial \tau} \mathbf{E} \mathbf{a}_i = \frac{1}{\tau} \mathbf{\Gamma} \mathbf{a}_i + (\mathbf{\Gamma} - \omega_i^2 \mathbf{E}) \frac{\partial \mathbf{a}_i}{\partial \tau}, \tag{3.20}$$

where the derivatives of $\mathbf{E}$ and $\mathbf{\Gamma}$ have been computed from Eqs. (3.9) and (3.10). The second term on the right vanishes if the equation is multiplied by $\mathbf{a}_i^T$ from the left (take the transpose of Eq. (3.19) and recall that $\mathbf{E}$ and $\mathbf{\Gamma}$ are symmetric), leaving

$$\frac{\partial \omega_i}{\partial \tau} = \frac{\mathbf{a}_i^T \mathbf{\Gamma} \mathbf{a}_i}{2\omega_i \tau \mathbf{a}_i^T \mathbf{E} \mathbf{a}_i}, \tag{3.21}$$

or

$$\frac{\partial f_i}{\partial \tau} = \frac{\mathbf{a}_i^T \mathbf{\Gamma} \mathbf{a}_i}{8\pi^2 f_i \mathbf{a}_i^T \mathbf{E} \mathbf{a}_i}. \tag{3.22}$$

The frequency derivatives calculated from Eq. (3.22) feed into Eqs. (3.17) and

(3.18), that in turn are used to find $\delta\tau$ in Eq. (3.16). Thus an iteration is complete and the incrementally better guess for the elastic constant (in one dimension) is $\tau + \delta\tau$. For a three-dimensional, homogeneous, isotropic sample, there are two elastic constants. The calculations to minimize χ^2 are more complicated, but follow the same basic procedure. Modern minimization procedures for RUS often allow variations in dimension as well as elastic constants [31].

Once the computational minimization procedure has been completed, there are several practical rules used in the RUS community to determine whether a particular frequency fit is valid or not. For example, at least five resonances should be measured and fit for each elastic constant desired, i.e., for an isotropic sample, a minimum of ten resonances should be used. Also, to consider a fit valid for a particular sample, the rms error ($\sqrt{\chi^2/N}$) should be less than 0.5% and each calculated resonance frequency should be within 2% of the corresponding measured frequency.

3.4 Resonance Frequency Measurements

The previous sections describe the process for deriving elastic constants from a set of resonance frequencies of a sample. This section gives a general overview of the process for measuring the resonance frequencies needed for analysis. Ideally, the measured resonance frequencies will include the lowest resonant mode and the next twenty or more consecutive resonances of a sample with free boundaries. In practice, the sample is held between two transducers that provide the frequency

excitation and detect the sample response as a function of frequency. This has two consequences: transducer contact compromises the free boundary assumption of the analysis, and transducer position influences which resonant modes can be excited and detected. The most common way to overcome these difficulties is to balance a sample on edges or corners between transducers, since the edges and corners then have minimal arial contact with the transducers and they are low symmetry locations (they are not nodal locations for most resonant modes).

Rectangular parallelepiped shaped samples are generally held between transducers on diagonally opposite corners for RUS measurements. However, for this work, corner-to-corner mounting proved impractical. As will be described later, the mounted sample and sample stage had to be lowered approximately 130 cm into a cryostat, and any jiggle easily knocked the sample free of its mount. Additionally, lanthanides are fairly soft metals and the polished corners and edges of samples are easily damaged. Thus, for these measurements, rectangular parallelepiped-shaped samples were mounted face to face between transducers. Figure 3.1 is a photograph of the sample stage with a small sample between two transducers.

In this set up, despite the flat mounting of the sample, a weak point contact between the sample surface and the transducers was achieved most of the time, since the transducers were slightly non parallel to each other. Due to varying sizes and densities, different materials were scanned over different frequency ranges: Gd from 200 to 400 kHz and Yb from 140 to 305 kHz. Between samples, a reference sample of lead (Pb) was also scanned from 150 to 350 kHz to check the system

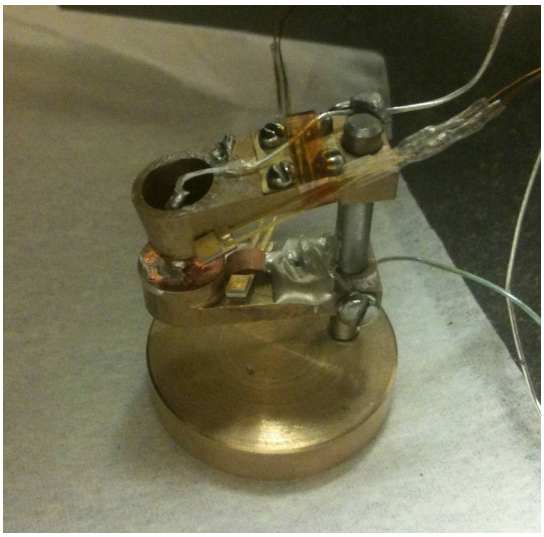

Figure 3.1: Sample stage. A small rectangular parallelepiped sample is held on opposite faces by two transducers. Note that the top transducer is attached to a hinged arm.

reliability.

During a RUS experimental measurement, a large amplitude response is detected by the receiving transducer when a match occurs between the frequency of the driving transducer and a natural frequency of the sample (an eigenfrequency). After each sweep over a specified frequency range, a chart display of the response amplitude versus frequency is obtained. A section of a real time spectrum is shown in Figure 3.2. The desired data is a list of resonance frequencies picked from the spectrum. This picking is done with a combination of user intelligence, Lorentzian fitting software, and the help of a *Labview*$^{\text{TM}}$ program. Once the sample resonances are determined, the elastic constants can be calculated using the previously explained error minimization procedure, or the frequencies may be displayed graphically to elucidate important trends or shifts.

A fundamental relationship between resonance frequency and material

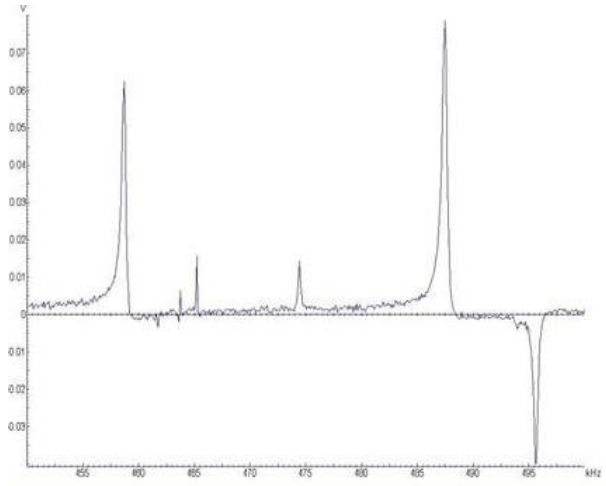

Figure 3.2: Representative frequency spectrum. Amplitude (arbitrary units) versus frequency (kHz) resulting from a RUS scan. The resonant frequencies are the peaks. Amplitude varies between resonances because different modes excite the region of the receiver differently.

modulus is through a speed of sound in the material, i.e., $f\lambda = v$, where λ is the wavelength of the standing wave and $v = \sqrt{\text{Elastic modulus/Density}}$ (see also Eq. (3.8) and the discussion of its solution). Thus, measured resonance frequencies are closely related to the square-root of some combination of elastic constants (c_{ij}s). Any shift in resonance frequency as a function of temperature or pressure is an indication of a shift in one or more elastic constant (modulus) of the material. Likewise, discontinuities in the resonance frequencies as a function of temperature or pressure indicate discontinuities in the moduli, which is a signature of a change in crystal structure or magnetic behavior. Therefore, characteristic changes in a material may be derived from high precision measurements of resonance frequencies as a function of temperature or pressure, without having to determine the elastic constants [24]. The frequencies measured for this research were sometimes, but not always, processed to derive elastic constants. Quite often, the important physics is

displayed in the frequency trends alone.

Chapter 4

Experimental Development

This chapter provides a detailed overview of the methods employed to perform RUS measurements on samples at temperatures between 77 K and 330 K. The essential steps are described in several sections: sample preparation, experimental chamber design, RUS sample stage, and electronics and data acquisition.

4.1 Sample Preparation

Sample preparation is a very critical part of any RUS related experiment. Although the techniques of sample preparation vary between laboratories, the purpose is always the same: to make a geometrically perfect sample with a minimum of defects. In practice, this means that sample preparation is often the most difficult and time consuming portion of a successful RUS experiment.

The samples prepared in this work were made from Gd and Yb polycrystalline specimens of high purity (99.9%) that were purchased from the

Alfa-Aesar Company. The gadolinium came in the form of a rod of 6.35 mm diameter and 50 mm length. The ytterbium came in the form of ingots. Photographs of the Gd and Yb specimens before the sample preparation process are shown in Figure 4.1. The goal was to create pristine rectangular parallelepiped (RPR) samples with sides $a \times b \times c$ of length between 0.3 cm and 0.4 cm and $a \neq b \neq c$.

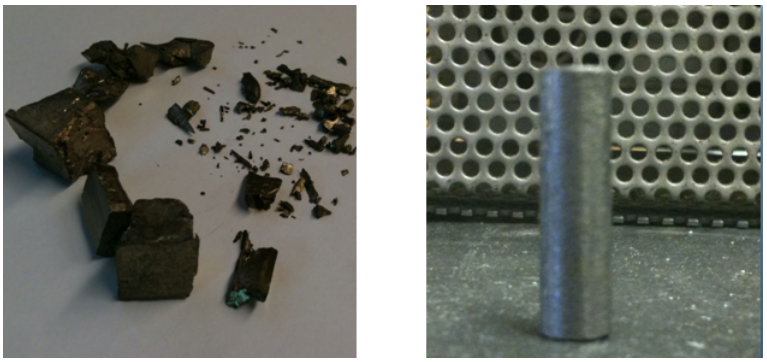

Figure 4.1: Lanthanide specimens before sample preparation. Left are Yb ingots, right is a Gd rod.

Initially, a diamond saw was used to cut rough parallelepiped shapes approximately 25% larger than the planned final dimensions. For the cutting process, the samples were secured to the cutting platform using a bonding agent as an adhesive. Because the materials used in this work oxidize in air, they were immersed in mineral oil during the entire cutting process. After cutting, acetone was used to dissolve the bonding agent. Plastic tweezers were used to remove the rough cut samples and soak them in an acetone bath followed by an alcohol bath. Photographs of the cutting system are shown in Figure 4.2.

The goal from this point forward was to produce perfect and scratch free parallelepiped samples through polishing. The polishing equipment included an

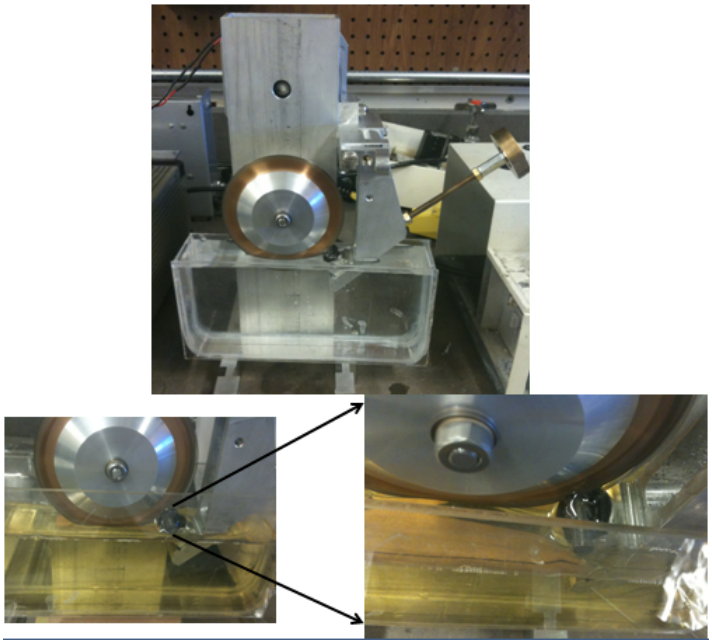

Figure 4.2: Cutting system.

Ultra Tech polishing wheel, several Buehler Petrographic slides, various sizes of polishing papers, crystalbond, a Thermolyne Type 1900 hot plate, a glass plate, a magnet and some gauge blocks.

Each rough sample was glued to a piece of petrographic slide, Figure 4.3, using crystal bond which is hard at room temperature but melts at 60° C. Crystal bond chips were placed over the sample and the slide with the sample was placed on the hot plate. The slide and the sample were then removed from the hot plate and allowed to cool. Once they cooled, the slide was placed on the polishing wheel, as shown in Figure 4.4. The sample was polished using silicon carbide papers of decreasing grit sizes until the crystal bond was removed and the sample had a mirror-like face. The same procedure was applied for all six faces. When scratches or surface defects appeared, the polishing paper was replaced with a larger grit paper and the process of decreasing the size was repeated.

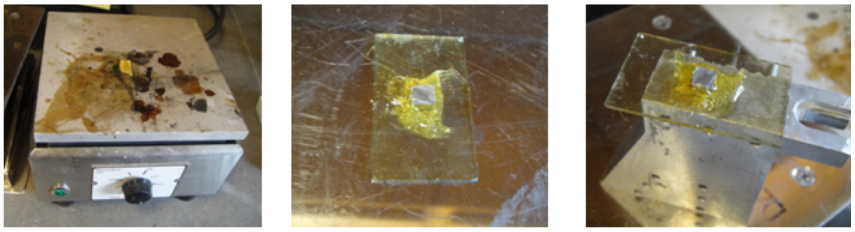

Figure 4.3: Preparing the sample for polishing process.

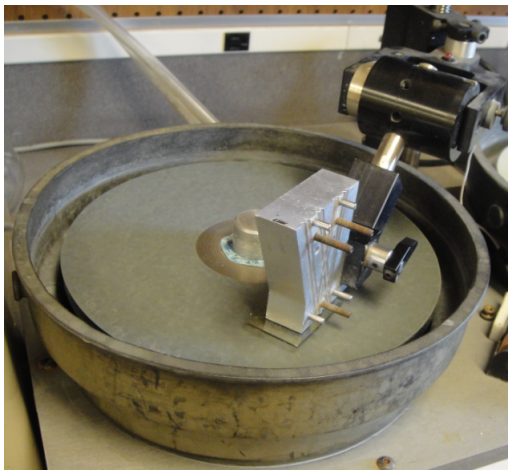

Figure 4.4: Photograph of the polishing wheel.

After the initial polished surfaces were obtained, right angle blocks were used to produce a right angle parallelepiped shape. The right angle blocks were attached to the polishing platform and the sample was trapped between the blocks using crystal bond, as shown in Figure 4.5. The polishing process was then repeated as described previously. When one face was completed, the sample was rotated so that it became a flat surface for the next side. This procedure was repeated until all 6 faces were perpendicular. After this, the sample was cleaned well in an acetone bath followed by an alcohol bath. At various points during the polishing process, the condition of the sample surface was checked using a microscope. A final version of one of the samples is shown in Figure 4.6.

Figure 4.5: Photograph of the polishing platform with right angle blocks.

Figure 4.6: A photograph of a completed parallelepiped Gd sample.

4.2 Experimental Chamber Design

The experimental chamber design was influenced by the shape of an available dewar. This dewar, shown in Figure 4.7, is a CSM-60 series stainless steel dewar manufactured by Cryofab Inc. It has double insulated walls, with space provided for an outer reservoir of liquid nitrogen and an inner reservoir of liquid helium. The central chamber available to hold the experimental apparatus is 40" deep and 10" in diameter.

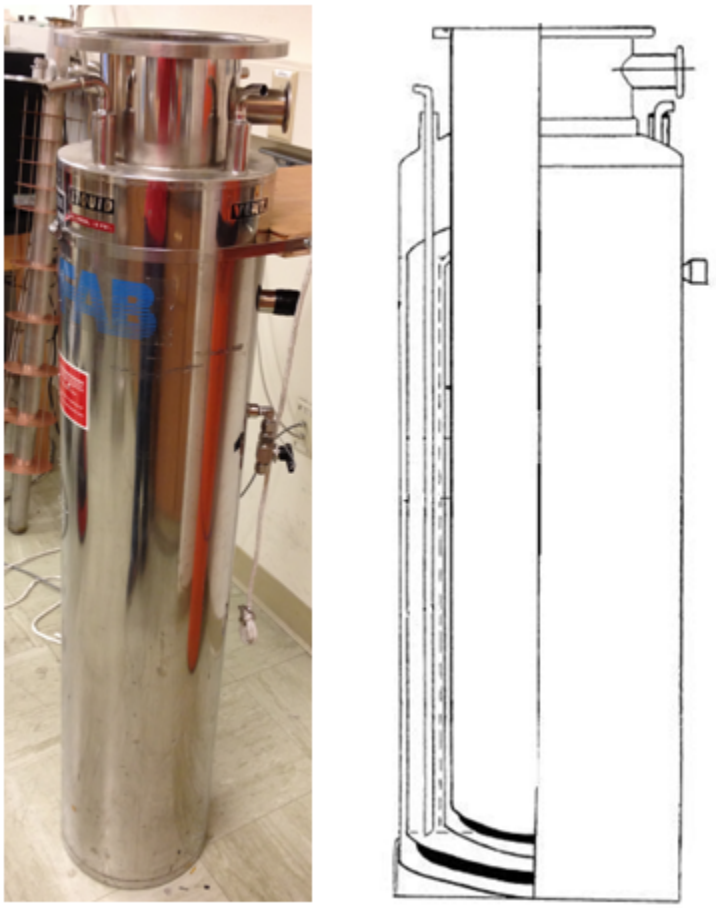

Figure 4.7: Left side: Photograph of the dewar that houses the experiment. Right side: Cross-sectional sketch of the dewar.

The contents of the dewar were designed by the author using Pro-E

software, and machined by the Physics Department Development Technician Wade Cline. An external radiation buffer column, shown in Figure 4.8, fills the outer part of the central dewar chamber. It consists of a hollow 2-inch diameter stainless steel tube and several 6-inch diameter copper plates soldered at regular intervals to the outside of the stainless steel tube. The purpose of the radiation baffles (copper plates) is to minimize the temperature difference between the top and the bottom of the system. A larger steel plate at the top of the radiation buffer column is the seal at the top of the dewar.

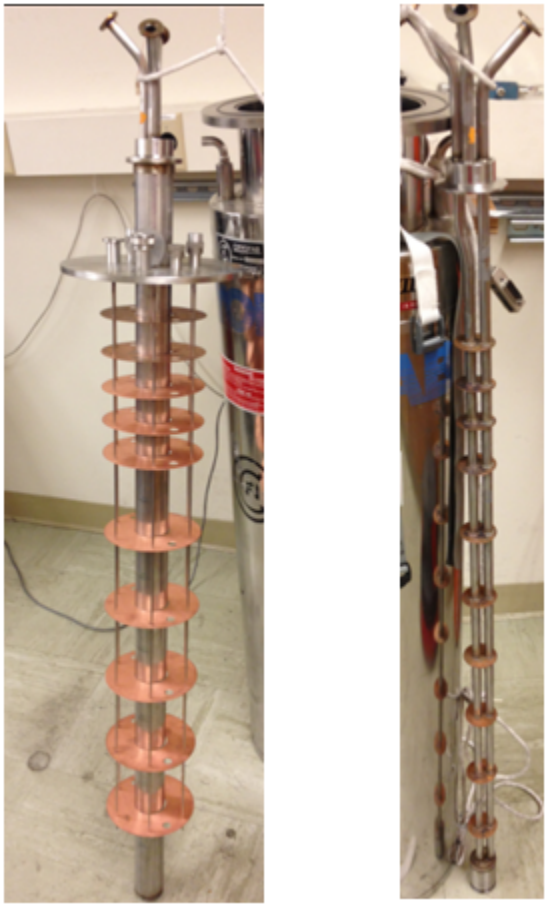

Figure 4.8: Left: A photograph of the radiation buffer column with the radiation baffles. Right: A photograph of the sample column with the sample chamber at the bottom.

The central sample column, Figure 4.8, slides into the 2-inch diameter stainless steel tube of the radiation buffer column. It consists of two 1/2-inch diameter hollow steel tubes 38 inches long, held vertical by 1.5-inch diameter copper radiation baffles soldered at equal intervals to reduce heat flow and liquid evaporation. The tubes are connected at the bottom to the sample chamber and act as the conduits for electronic cables, gas, and vacuum feeds from outside the dewar.

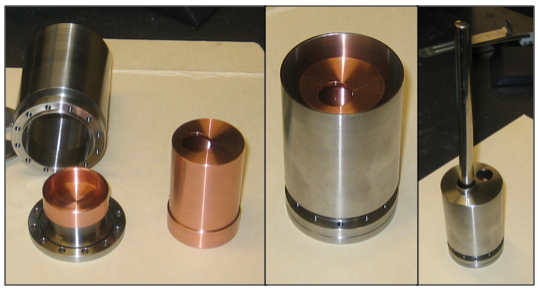

Figure 4.9: A photograph of the sample chamber parts: copper pot, copper stage, steel pot and steel tubes.

The sample chamber is shown in Figure 4.9. It consists of an internal copper pot around which a pair of twisted copper wires is wrapped for heating (Figure 4.10), and an external stainless steel pot. The copper pot is soldered into the stainless steel pot with the heating wire filling the space between them. Two silicon diode thermometers inside the copper pot provide temperature sensing during heating and cooling cycles.

4.3 RUS Sample Stage

Photographs of the RUS sample stage are shown in Figs. 3.1 and 4.11. Two brass arms are attached to an aluminum post, supported by a brass platform. The lower

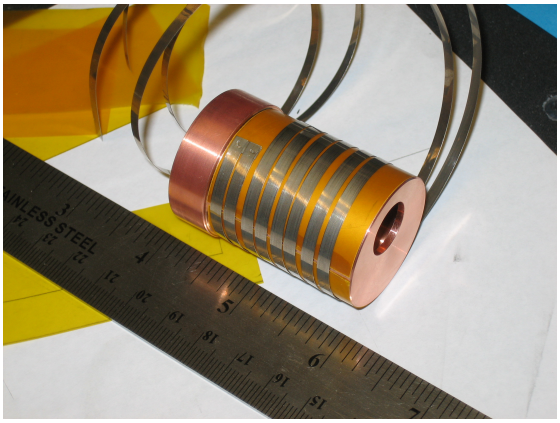

Figure 4.10: The copper chamber wrapped with a twisted pair of copper wires for heat conduction.

brass arm is a fixed platform, while the upper brass arm is hinged to allow easy placement of samples and a gravitationally assisted mount for the samples. A cored cylinder, similar to the body of a drum, is at the end of each brass arm. The aluminum stage and brass arms were machined by Wade Cline in the physics machine shop. The author built the transducer assemblies as described below.

Figure 4.11: Photo of brass transducer stage arms and platform. Two sets of arms were built, as shown. Only one set was used during a particular experiment.

Kapton films provided the drumhead covering for the inner sides of the cored cylinders on the brass arms. The kapton films act as acoustic insulators, preventing coupling of sound through the brass arms and aluminum platform. A

slip fit hole was made on each kapton film to hold the piezoelectric disks used as transducers. The piezoelectric disks were attached to the kapton, and the kapton was attached to the cored cylinders, using Emerson and Cuming Stycast 1266 epoxy which is clear, has low viscosity, is room temperature curable and has good impact strength, good moisture resistance and good electrical properties.

A copper film was deposited over the top surface of the transducers to act as the ground connection for the transducers. Vacuum thermal evaporation was the deposition technique: A copper source was placed inside a vacuum chamber with the transducer assembly to be coated, and heated until its surface evaporated. The evaporated material condensed onto the colder substrate surface, forming a thin film. The vacuum chamber held a pressure of 10^{-6} to 10^{-5} Torr, to avoid reaction between the vapor and atmosphere. At these low pressures, the mean free path of vapor atoms is the same order of magnitude as the vacuum chamber dimensions, so evaporated particles travel in straight lines from the evaporation source to the substrate to create an even coating. The copper film surfaces were checked using the scotch tape test: if no coating comes away with applied scotch tape, the coating is acceptable.

After the coating process, a short metalized strip of kapton (also coated with copper) was attached on the center of the back side of each transducer using MG Chemicals Silver conductive epoxy (due to its high electrical conductivity and strong conductive bonding). The metallization on the kapton strips provides electrical leads to the transducers. On the other end of the metallized strip centers,

coaxial center conductors were attached using silver epoxy. The braid of the coaxial cable was attached onto the copper coated face of the transducer assembly, also using silver epoxy. Connecting the coaxial to the transducer was highly delicate work due to the small area of the transducer and kapton film. Once both transducers were prepared, the brass arms were attached to the aluminium platform using small screws.

4.4 Electronics and Data Acquisition

The electronics to control the temperature and obtain accurate resonance data included a Stanford SRS 844 two-phase lock-in amplifier, a Stanford DS 345 function generator, a Lakeshore PID temperature controller TC 330, and a power supply to warm up the system. The input signal was generated by the DS 345 driving one of the transducers (the driver). The output from the other transducer (the receiver), which included the resonant signal, noise and any other interference, was collected by the SRS 844. The raw signal to the SRS 844 was in sinusoidal form with a frequency equal to the drive frequency and an amplitude dependent on the background noise. The SRS 844 split this input signal into two. It multiplied one by a reference signal directly from the DS 345 producing the in-phase channel value. The second signal was multiplied by the reference signal phase shifted by $\pi/2$ producing the quadrature channel value. Amplitude and phase were calculated from these.

To control the temperature in the apparatus, liquid nitrogen (LN) was

used for active cooling and a power supply (max 10 V and 30 Amp) was used for heating. The power supply was connected to the heater coil using a bnc cable and a banana plug. The PID TC 330 was connected to two calibrated silicon diode thermocouples to record temperature. One thermocouple was placed very close to the sample in the RUS cell, while the other was placed at the chamber wall.

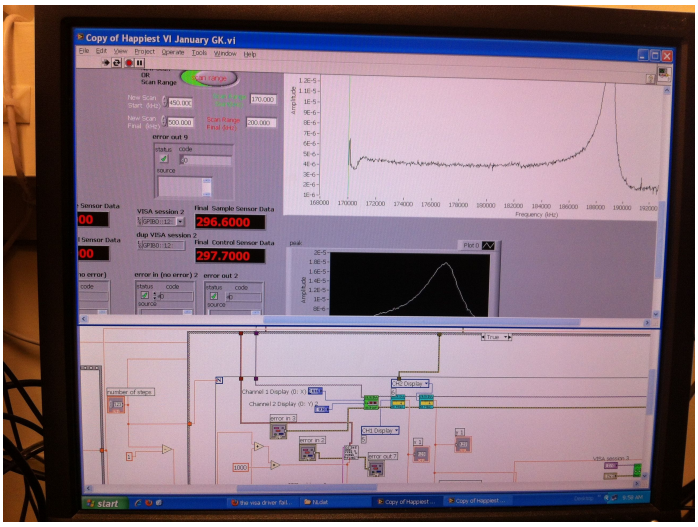

Figure 4.12: Labview interface to control the electronics and the experiment.

A $LabView^{TM}$ interface, Figure 4.12, was written to control and read out the lock-in amplifier and function generator of the RUS system, to interface the cryostat temperature controller and to acquire data. The main program allows the user to set the amplitude of the stimulus signal, the frequency range of the measurement and the frequency sweeping step. For the samples studied here, a frequency range of 200 kHz - 400 kHz for Gd and 100 kHz - 200 kHz for Yb covered the 20 lowest resonance frequencies. The frequency step was set such that 1024 data points were taken over the frequency range.

An experimental run began at room temperature. The addition of LN to

the dewar very quickly reduced the sample chamber temperature to approximately 80 K. As the LN evaporated and temperature increased, frequency spectra were continuously measured over the set frequency range, sweeping from low to high frequency. A text file with various columns was generated for each spectrum where frequency, amplitude, signal in-phase, signal out-of-phase, and the two thermocouple temperature readings were recorded. Header material included the date and time, start and finish frequencies, initial and final temperatures. Each scan took approximately two minutes to generate and record. After one scan ended, a new scan began immediately. For data analysis, the initial text files were converted into the DRS file format so that individual peaks could be interpreted with the help of the DRS resonance fitting program. Details on the analysis of the peaks and the DRS fitting program are given in the next chapter.

Chapter 5

Experimental Results

The goal of these experiments was to explore the physical phase space and elastic behavior of two lanthanides as a function of temperature at ambient pressure. The experimental method of exploration involves tracking resonance frequency behavior as a function of temperature. A discontinuity or abrupt change in slope in resonant frequency versus temperature is indicative of a phase change, either structural or magnetic. The slope of frequency versus temperature indicates the trend of the elastic behavior: increasing frequency correlates with hardening, decreasing frequency correlates with softening

Experiments were carried out on two test samples, stainless steel (SS) and lead (Pb), and three lanthanide samples, one of gadolinium (Gd) and two of ytterbium (Yb-1 and Yb-2). The dimensions and masses of the samples are shown in Table 5.1. Table 5.2 shows the order and descriptor of experiments. Resonance frequency spectra, similar to the spectrum shown in Figure 3.2, were collected as a

sample	mass (g)	d1 (cm)	d2 (cm)	d3 (cm)
SS	0.8928	0.5130	0.4865	0.4610
Pb	0.3793	0.3654	0.3230	0.2986
Gd	0.3429	0.36027	0.34820	0.34625
Yb-1	0.3030	0.41630	0.34320	0.30410
Yb-2	0.3807	0.52915	0.33605	0.30690

Table 5.1: Experimental sample labels, masses, and parallelepiped dimensions.

function of temperature in the range 10 - 350 K. For each sample, RUS measurements were carried out (spectra were collected) as the sample was cooled or warmed and then returned to room temperature. Temperature protocols were repeated and then varied to explore interesting temperature regions and behaviors. Each RUS scan of frequency versus amplitude took approximately two minutes to complete, during which the temperature may have changed by 2.5 - 3.5 K on cooling and 1 - 1.5 K on heating. The saved output is a text file recording frequency, amplitude, temperature, and signal phase. Figure 5.1 shows the header and first lines of a typical output file. Key resonances were picked from the spectra and tracked over time (corresponding to temperature). In the following sections, the results for each sample are discussed in more detail.

5.1 Stainless Steel Sample, System Test

The first comprehensive test of the experimental system was made using a polycrystalline stainless steel sample. Stainless steel was chosen for two reasons. First, stainless steel is easy to obtain and (importantly for resonance tests) has low dissipation (high Q) and thus very sharp resonances. Its resonance frequencies are

Dates	**Sample**	**Descriptor**	
July 2011	SS	transducer test	
Aug - Sept 2011	Gd	Run 1	
		Run 2	
		Run 3	
December 2011	Yb-1	Run 1	Cycle 1
			Cycle 2
			Cycle 3
January 2012	Yb-1	Run 2	Cycle 1
			Cycle 2
			Cycle 3
March 2012	Yb-1	Run 3	
March 2012	Pb	system test 1	
March 2012	Yb-2	Run 1	
Nov - Dec 2012	Yb-1	Run 4	Cycle 1
			Cycle 2
			Cycle 3
			Cycle 4
December 2012	Pb	system test 2	
December 2012	Yb-2	Run 2	Cycle 1
			Cycle 2
			Cycle 3
January 2013	Yb-2	Run 3	Cycle 1
			Cycle 2

Table 5.2: Order of experiments on the samples. Between runs, the sample was removed from the sample chamber and reset between the sample stage transducers. During a cycle, the temperature was varied in a predetermined way and then allowed to settle back to room temperature before the next cycle.

Date and Time (H:M:S):	Aug 29 2011 13:00:54		
Number of Points:	1024		
Start frequency (kHZ):	200		
Final frequency (kHZ):	400.029412		
Initial Temp:	139.6		
Final Temp:	136.76		
Freq (Hz)	**Amplitude**	**T sample**	**Phase Theta (Deg)**
200000.00	0.00	139.60	0.00
200195.53	0.00	139.57	1.57
200391.06	0.00	139.55	-1.32
200586.60	0.00	139.55	-1.31
200782.13	0.00	139.54	-1.31
200977.66	0.00	139.54	-1.29
201173.19	0.00	139.54	-1.31
201368.73	0.00	139.54	-1.31
201564.26	0.00	139.54	-1.27
201759.79	0.00	139.53	-1.29
201955.32	0.00	139.53	-1.31
202150.85	0.00	139.53	-1.30

Figure 5.1: Example top portion of a saved output text file.

easily distinguishable both from the background and from the each other. Second, it is often easier to find something if you know where to look. This sample was previously studied by other researchers in the lab. Thus, forward calculations of its resonances and room temperature measurements had been made and recorded. Given the previous experimental measurements, the SS sample could be used as a standard to test the functioning of the handmade transducers.

RUS measurements were performed twice: once using the LabVIEW program developed to control the system under temperature variation; once with a commercial controller (DRS box) that was designed specifically for RUS measurements, but does not have the flexibility to control complex experimental configurations. Spectra were obtained in the frequency range 275 - 900 kHz for each test. A section of the spectrum for each test is shown in Figure 5.2. The transducers clearly transmitted and received high quality signals, and the two resonance control

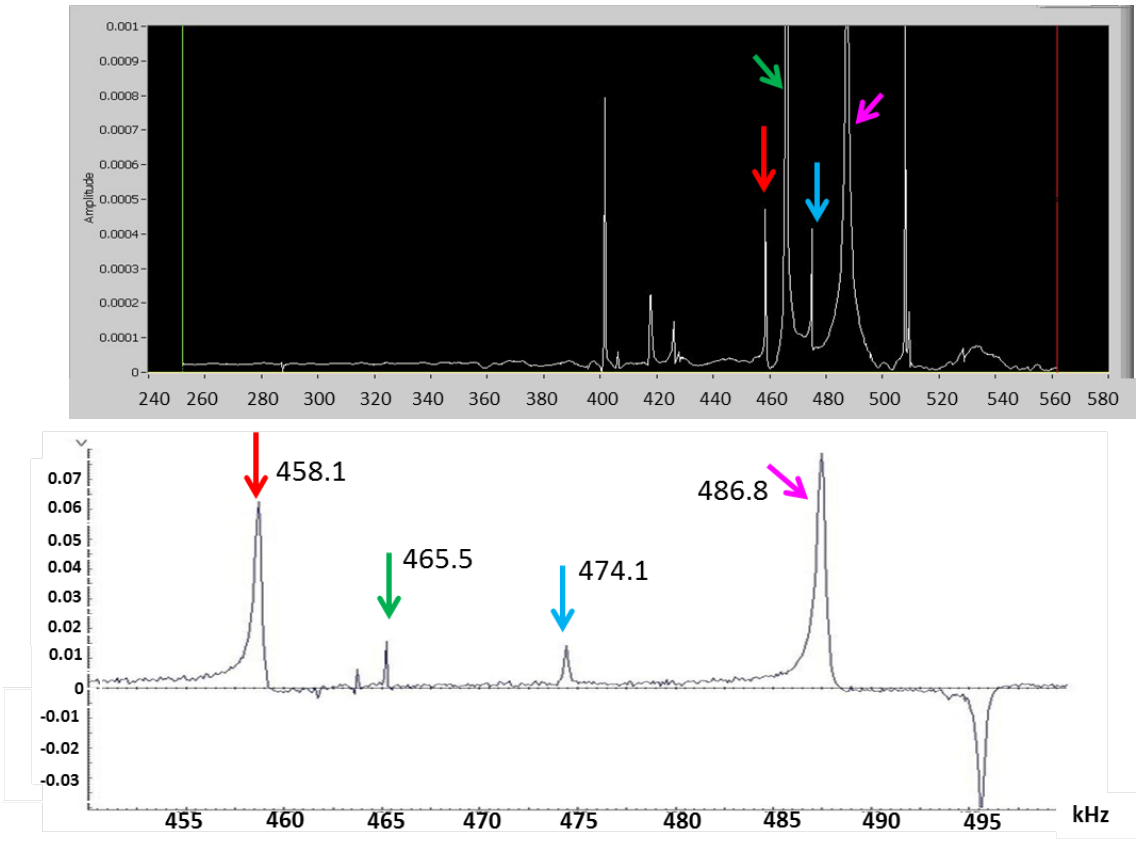

Figure 5.2: Steel spectra taken using the Labview control system developed in this work and a commercial DRS box. The horizontal axis is frequency in kilohertz; the vertical axis is (arbitrary) amplitude. Some common frequencies are indicated.

systems produced similar results. Between experiments, the SS sample was reset between the transducers; thus, the points of contact and the excited and detected resonances varied between the two measurements. However, at least ten resonances are clearly common to both tests. Table 5.3 shows a the expected and measured resonance frequencies between 275 and 605 kHz. The transducers work well with both system controllers. Frequencies are measured in MHz to six decimal digits, and converted to kHz in the data displayed in this document. The variations in frequencies obtained by the various calculation and measurement methods are less than 1%.

Calculated	**LabVIEW**	**DRS box**
288.0	287.8	287.2
323.9	323.5	323.8
390.7	388.3	388.4
401.7	400.9	400.9
408.8	405.4	405.6
419.6	417.5	417.6
427.4	425.6	425.6
429.5	427.5	427.8
460.8	458.1	458.2
468.4	465.2	465.5
475.5	474.1	474.0
489.2	486.9	486.8
494.6	493.1	494.0
496.5	495.1	495.4
509.7	507.4	507.8
510.7	508.8	509.2
530.1	528.1	530.1
565.6	565.2	565.4
573.0	572.2	572.8
585.7	582.9	
590.0	587.0	588.7
593.0	591.8	592.3
602.0	602.2	602.2

Table 5.3: Room temperature resonance frequencies of a stainless steel sample. The columns are the calculated (expected) resonance frequencies, the frequencies measured using the handmade transducers with a program developed in LabVIEW, and the frequencies measured using the handmade transducers with a commercial DRS box. Blank cells are missing frequencies.

5.2 Gd Sample

Three experimental runs were performed on the gadolinium sample. Between experimental runs, the sample was extracted from the sample chamber and re-set between the transducers. During each run, the sample was cooled from room temperature to 80 - 90 K by slowly filling the liquid nitrogen reservoir of the dewar. Cooling took approximately three hours thirty minutes, resulting in nearly 70 RUS spectra. The sample returned to room temperature through ambient heating over 48 hours, resulting in more than 200 RUS spectra. Each RUS spectrum consists of data at 1024 frequencies in the range 200 - 400 kHz. This frequency range covers the first 20 resonances of Gd, as predicted by a forward calculation of resonance frequencies, given the sample's physical characteristics (Section 3.2). Table 5.4 shows the temperature extremes for each experimental run. Because the warming periods were very long, they often ran over night. Then, when there were technical difficulties in the middle of the night, data was lost over significant temperature ranges. This is the case for Run 1 between 243 K and room temperature and all of the warming part of Run 2. During the warming phase of Run 3, the heater coil was employed to heat to 319 K for the first and only time on this sample.

A typical frequency spectrum is shown in Figure 5.3. Figure 5.4 shows a spectrum of resonances between 275 - 375 kHz at 298 K and 227 K (measured in the third run). A first look through all of the collected spectra showed that a set of resonance frequencies between 336 and 357 kHz at room temperature (shown in Figure 5.5) are consistently easy to spot, pick, and track. These frequencies are the

Run	Trend	Initial T (K)	Final T (K)
1	Cooling	295	90
	Warming	90	243
2	Cooling	296	90
3	Cooling	298	80
	Warming	92	319

Table 5.4: Temperature extremes during experimental runs on Gd. RUS spectra were obtained between the initial and final temperatures listed. Technical problems caused the loss of warming data for Run 2 and part of Run 1.

9th - 14th resonances of the sample, according to the forward calculation as described in Section 3.2. The predicted resonances for $T = 297$ K and their dependence on the two elastic constants, c_{11} and c_{44} (see Section 3.1), are shown in Table 5.5. Notice that three of the six resonances are pure shear in nature; thus the data should give a very reliable shear modulus ($c_{44} = \mu$). For each of the three runs, these resonances were tracked as a function of temperature and are shown in Figure 5.6. The first resonance could not be reliably picked from Run 2 and 3, probably because of the orientation of the sample between the transducers. Otherwise, there is a great deal of consistency between results of the experimental runs. The resonance frequencies in Figure 5.6 increase 3-5% as temperature decreases from 320 K to 80 K.

Figures 5.7 and 5.8 show Run 2 cooling resonance frequencies and normalized squared resonance frequencies. Lines connecting measured points have been added to guide the eye. The behavior of the pure shear squared resonance frequencies (Figure 5.8, the green and teal dots (11th and 13th resonances)) can be compared to measurements of the shear modulus, such as those shown in Figure 2.3

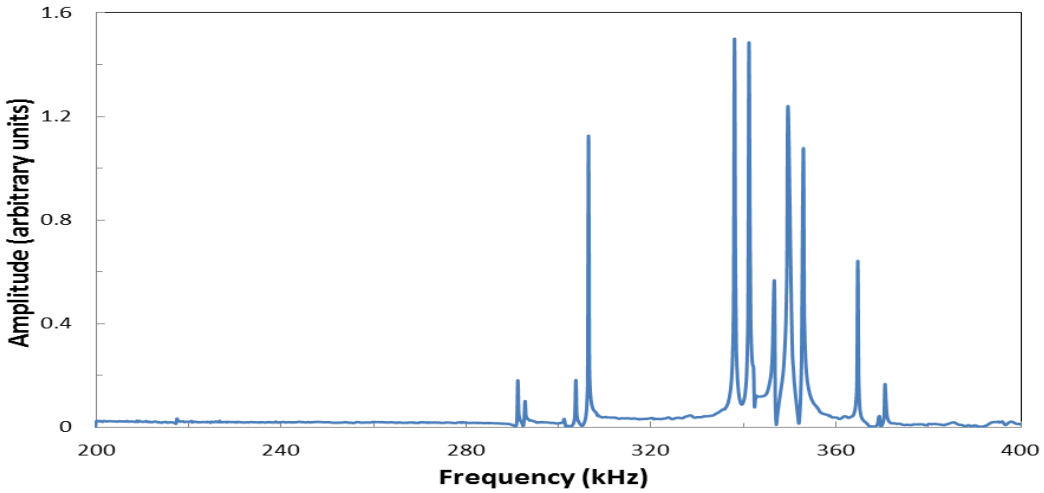

Figure 5.3: Room temperature frequency spectrum for Gd sample.

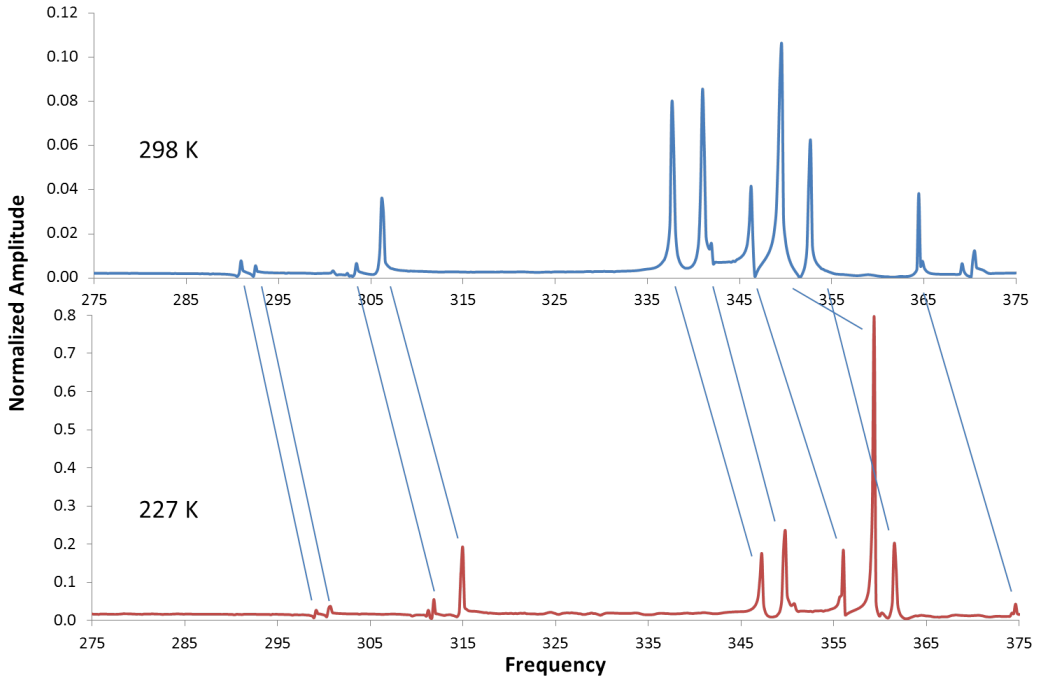

Figure 5.4: Gadolinium resonances at two temperatures during cooling in Run 3. As temperature decreases, resonance frequencies increase.

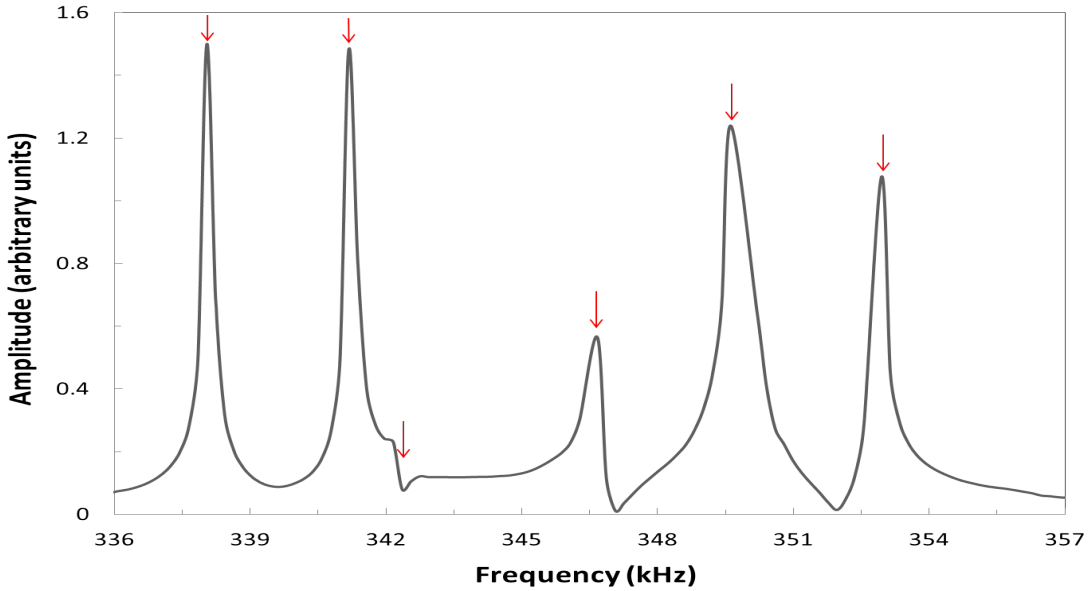

Figure 5.5: Close-up of Figure 5.3 showing the resonances between 336 and 357 kHz.

Resonance	**Frequency (kHz)**	% c_{11}	% c_{44}
9	338.0	0	100
10	341.0	42	58
11	342.4	0	100
12	346.0	42	58
13	349.1	0	100
14	352.7	42	58

Table 5.5: Predicted 9th - 14th resonant frequencies of Gd at $T = 297$ K. For each frequency, the involvement of elastic constants, c_{11} and c_{44}, in the resonance is shown.

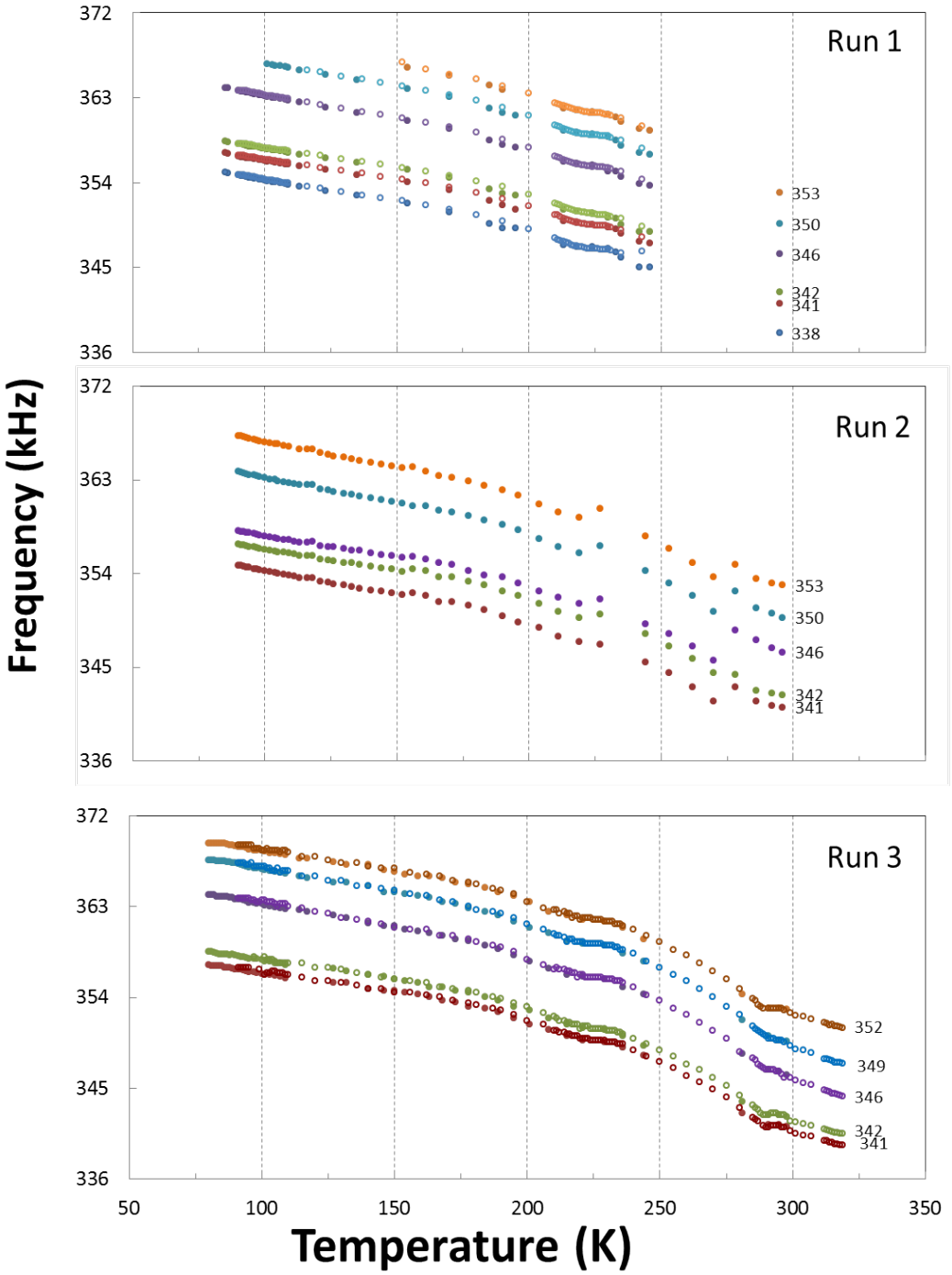

Figure 5.6: Gadolinium resonances as a function of temperature for Runs 1-3. Initial values of the frequencies are labeled. Solid circles are frequencies on cooling; open circles are frequencies on warming.

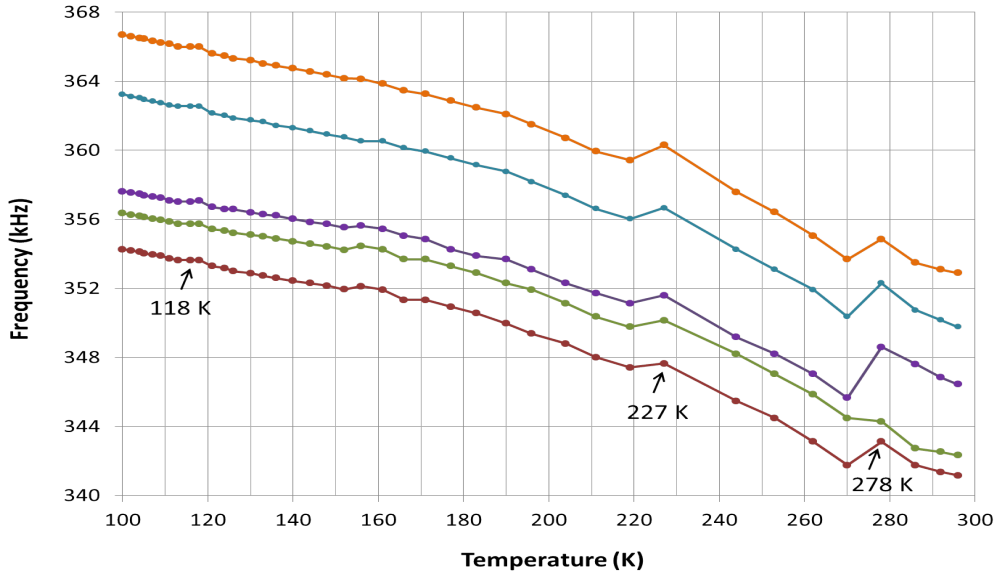

Figure 5.7: Resonance frequencies of Gd as a function of temperature, Run 2 cooling.

from Rosen[6]. Directly comparing figures, between 300 and 100 K, Rosen measured a change in elastic constants of 10%. Over the same temperature range, the Run 2 Gd squared resonance frequency changes by 8%.

Based on the studies of gadolinium discussed in Section 2.2, phase transition signatures should be apparent in the data at approximately 115 K, 224 K, and 292 K. In fact, three transitions are apparent in the resonance measurements where the trend of frequency versus temperature changes abruptly. For consistency, the highest resonance during an obvious transition is indicated on Figure 5.8. These frequencies indicate transitions around 118 K, 227 K, and 278 K. The lower two temperatures are consistent with Rosen's results and an accurate pick of the highest temperature transition may be compromised by the rapidly changing temperature during RUS spectra collection. There is also an interesting wiggle in some of the frequencies at around 160 K; however, it is not consistent between Runs, or even all

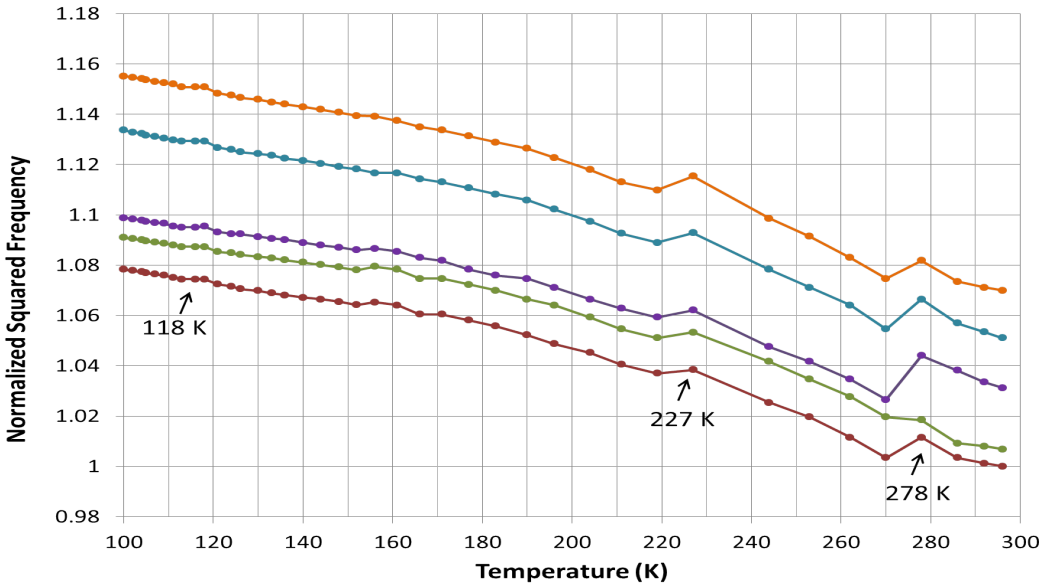

Figure 5.8: Normalized resonance frequencies squared of Gd as a function of temperature, Run 2 cooling.

frequencies in the same Run.

The Run 3 warming data have the most comprehensive temperature coverage of the experiments on gadolinium. In addition, a large number of characteristic resonance frequencies can be reliably picked from most of the RUS spectra. Thus, for Run 3 warming, the resonance frequencies can be inverted to find elastic constants (Section 3.3). The inversion software produces a best fit for elastic constants c_{11} and c_{44} as a function of temperature. These are related to the familiar shear modulus, Young modulus and compressibility by the relationships

$\mu = G = c_{44}$, $E = c_{44}(8c_{44} - 3c_{11})/(3c_{44} - c_{11})$, and $K_S = 1/(c_{11} - 4c_{44}/3)$

respectively. Figures 5.9 and 5.10 show the young's modulus, shear modulus, and compressibility for Run 3 warming. These figures are directly comparable to those published by Rosen[6] and shown in Figures 2.3 and 2.4.

The trend and magnitude of the shear modulus and the young's modulus calculated from resonances is similar to Rosen's results, although the results derived from resonance are approximately 5% higher in magnitude. Both Rosen's and the resonance-derived moduli decrease by 10% between 100 K and 300 K . Three of the four phase change signatures seen by Rosen are evident in the resonance-derived shear modulus as less-dramatic changes in slope than Rosen's. The fourth, at 15 K, is outside of the temperature range explored through resonance. As described in Section 2.2, Rosen's data show the Curie temperature of gadolinium $T_C = 292$ K, a spin reorientation temperature $T_{SR} = 224$ K, and a second spin reorientation temperature $T_R = 115$ K. The resonance-derived shear modulus slope changes are at approximately these temperatures.

Explicit transition temperatures derived from resonance data are much more dramatic in the compressibility, Figure 5.10. Here, T_C and T_R manifest themselves as step changes in the compressibility; T_{SR} is a much smaller, but very clear wiggle, on top of a smooth background. Choosing central points in each of these features, the data indicate $T_C = 289$ K, $T_{SR} = 222$ K, and $T_R = 116$ K. While the characteristic temperatures are similar to those recorded by Rosen, their manifestation in the data is quite different. The compressibility increases with temperature in both sets of data, Rosen's increasing by 5% between 100 K and 300 K; the resonance-derived compressibility increasing by 20%. Once again, the magnitudes are similar, although the resonance-derived values are higher. Table 5.6 shows the comparative values and the respective changes at 100 K and 300 K.

Reference	100 K	300 K	Change
Rosen [6]	2.490	2.6240	5%
Gunes	2.3419	2.8481	20%

Table 5.6: Compressibility values of gadolinium at 100 K and 300 K and percent changes.

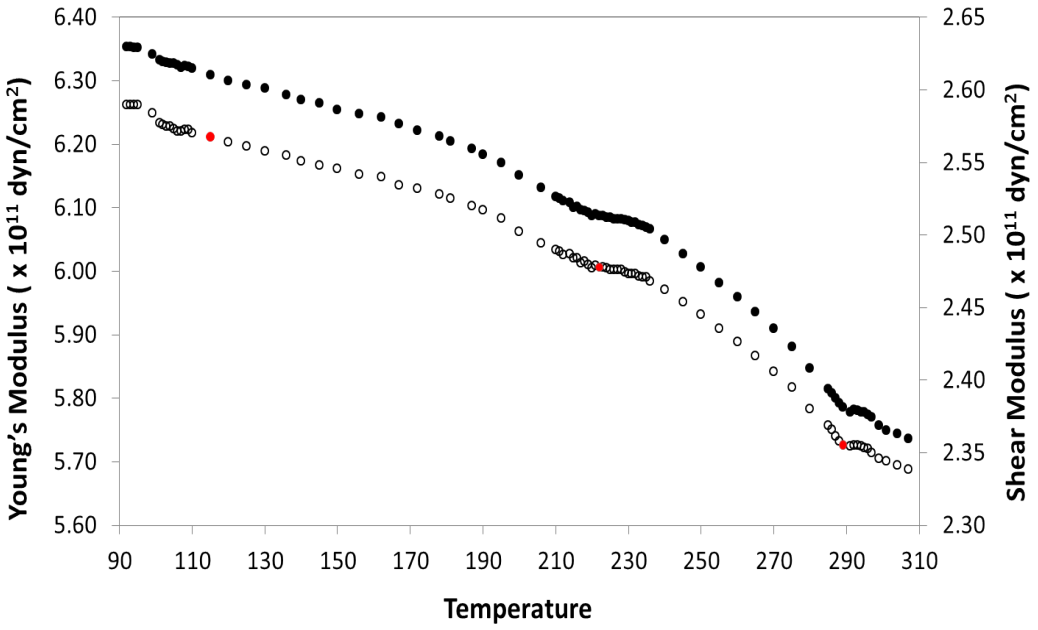

Figure 5.9: Shear modulus (c_{44}) (empty circles) and Young's modulus (solid circles) of Gd as a function of temperature, calculated from resonances picked from Run 3 warming spectra.Red circles indicate the transition points chosen from the Figure 5.10.

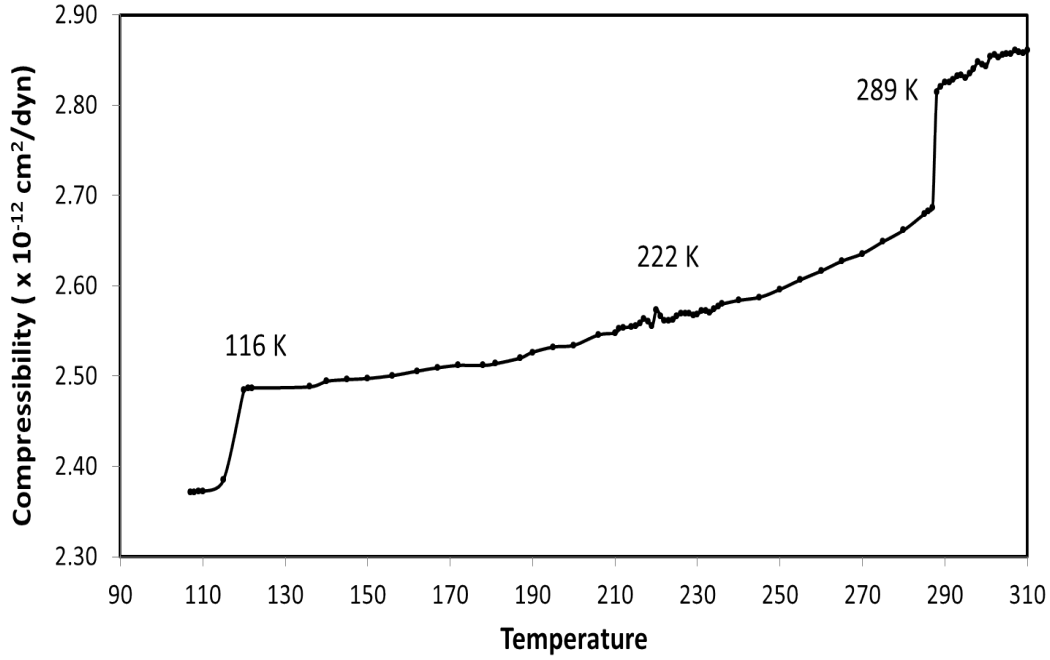

Figure 5.10: Compressibility as a function of temperature, from Gd Run 3 warming resonances.

A comparison of Figures 5.8 and 5.10 indicates that the magnetic behavior changes in gadolinium can occur over a range of temperatures, depending on conditions. The characteristic temperatures indicated in Figure 5.8 are found from resonance spectra taken as the system is cooled, while those in Figure 5.10 are from a warming experimental protocol. Rosen's measurements were "mostly carried out during the warm up from liquid-helium to room temperature" [6].

The behavior of the gadolinium sample is generally as expected from previous measurements using other techniques. Transitions manifest themselves as slope discontinuities in resonance frequency versus temperature. The resonance frequencies are a reliable indicator of the expected transitions, although a full inversion of the data to find elastic constants gives more robust indications of

Date	Run	Cycle	Trend	Initial T (K)	Final T (K)
December 2011	1	First	Cooling	294	121
			Warming	121	330
		Second	Cooling	330	281
			Warming	281	294
		Third	Cooling	297	135
			Warming	135	297
January 2012	2	First	Warming	297	342
			Cooling	342	234
			Warming	234	298
		Second	Warming	295	330
			Cooling	330	274
			Warming	274	290
		Third	Warming	295	340
			Cooling	340	281
		Fourth	Warming	281	344
			Cooling	344	277
			Warming	277	296
March 2012	3	First	Cooling	296	79
			Warming	N/A	N/A

Table 5.7: Temperature extremes during experimental runs on the Yb-1 sample.

transition temperatures.

5.3 Yb-1 Sample, Runs 1 - 3

Three consecutive experimental runs were performed on the Yb-1 sample, with the dates and temperature extremes shown in Table 5.7. The results of experiments on ytterbium were surprising, and thus each successive measurement inspired the next one. For maximum clarity of the experimental protocol and motivation, the experiments will be discussed in the order in which they occurred.

The expected room temperature resonance frequencies on Yb-1 were calculated and are shown in Table 5.8, along with the measured resonance

Resonance	Frequency (kHz)	Calculated (kHz)	% c_{11}	% c_{44}
1	112.8	111.9	0	100
2	148.8	148.0	13	87
3	155.2	154.6	15	85
4	158.6	158.2	0	100
5	171.0	171.6	2	98
6	182.6	182.8	2	98
7	188.4	187.1	5	95
8	194.4	196.2	3	97

Table 5.8: Predicted 1st - 8th resonance frequencies of Yb-1 at $T = 297$ K. For each frequency, the involvement of elastic constants, c_{11} and c_{44}, in the resonance is shown.

frequencies found in an initial scan over a large frequency range. It soon became apparent that many frequencies appeared inconsistently and the most consistent resonance was the seventh (188.4 kHz at room temperature). The seventh resonance was strong and easy to track through almost every temperature cycle, and is the focus of most of the discussions. In general, ytterbium is a softer material than gadolinium and is more difficult to explore using RUS.

5.3.1 Run 1

The first run of experiments on the sample had three cycles. In the first cycle, the sample was cooled from room temperature to 121 K by very slowly filling the liquid nitrogen reservoir of the experimental dewar (Figure 4.7) over three hours, resulting in 60 RUS spectra. After active cooling, the sample returned to room temperature through diffusive processes over 17 hours, and was then actively heated to 330 K using the heating coil wrapped around the sample chamber over 3.5 hours. The second cycle began at 330 K; the sample was actively cooled to 281 K and allowed to

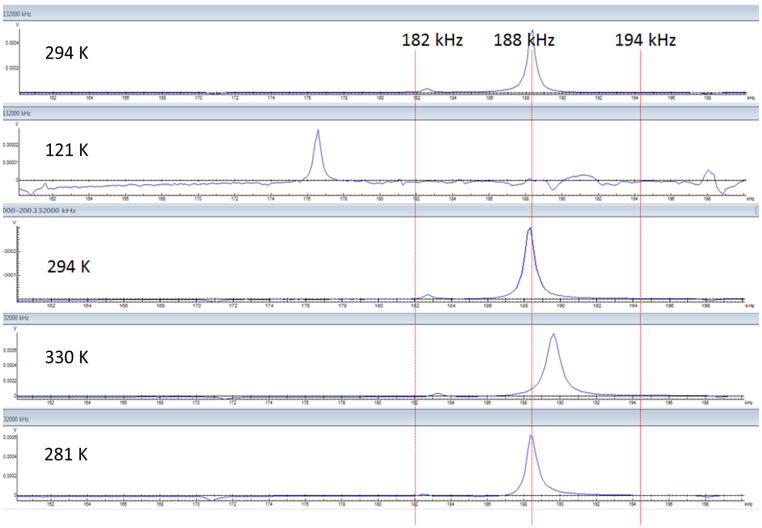

Figure 5.11: Response of the seventh resonance frequency of the Yb-1 sample at extreme temperatures during Run 1. The horizantal axis is the frequency (kHz), and vertical axis is the amplitude of the signal.

diffusively warm to room temperature. The third cycle was an active cool from room temperature and a diffusive warm, similar to the cycles performed on gadolinium. RUS spectra were measured continuously during each cycle. They consist of 1024 data points over the frequency range of 140-305 kHz. Figure 5.11 demonstrates the prominance of the seventh resonance at a variety of temperatures. Note that the sixth and eighth resonances are almost invisible on the scale of the seventh.

Figure 5.12 shows the temperature dependence of the seventh resonance during the first run. The overall positive slope is unexpected. As temperature decreases, the elastic moduli of most solids increases [36]. Resonance frequencies generally correlate with elasticity, so the expectation is to see frequency increase as temperature decreases, unless a phase transition is imminent. The hysteresis at high temperature is a signature of the martensitic transition discussed in Section 2.3. Ytterbium changes magnetic and physical structure at 310 K from a high

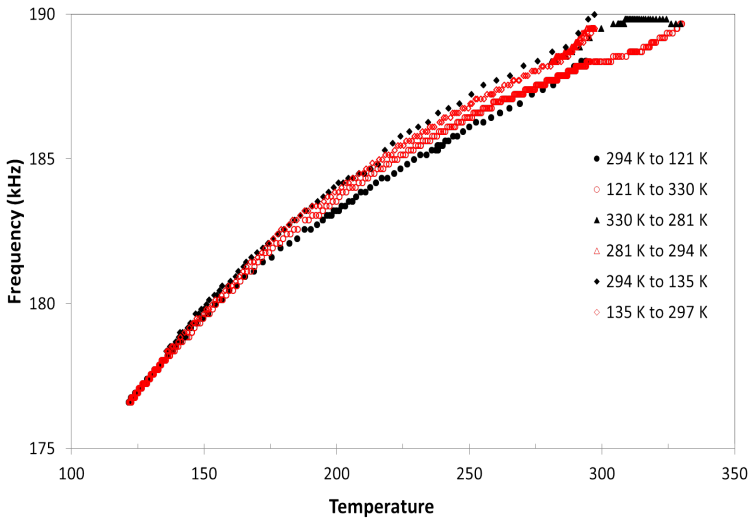

Figure 5.12: Evolution of the seventh resonance frequency of Yb-1 as a function of temperature during Run 1. The overall positive slope is a surprise. The hysteresis at high temperature is a signature of the martensitic transition between fcc paramagnetic and hcp diamagnetic structures (Section 2.3). Black circles are cooling and red circles are warming.

temperature paramagnetic fcc structure to a low temperature diamagnetic hcp structure [5]. The Run 1 data indicate hysteresis between 280 K and 330 K. This temperature region was explored further in Run 2.

5.3.2 Run 2

Between runs, the sample is always removed from the sample chamber and repositioned. Given the surprising results of Run 1, repositioning was deemed particularly important before Run 2. This would be the first test of whether results are repeatable. The plan for Run 2 was to explore the region of hysteresis in Run 1. Thus, the sample was actively heated above room temperature four times, cooled to temperatures below room temperature but above 230 K, and then allowed to return to room temperature. Figure 5.13 shows the four Run 2 cycles.

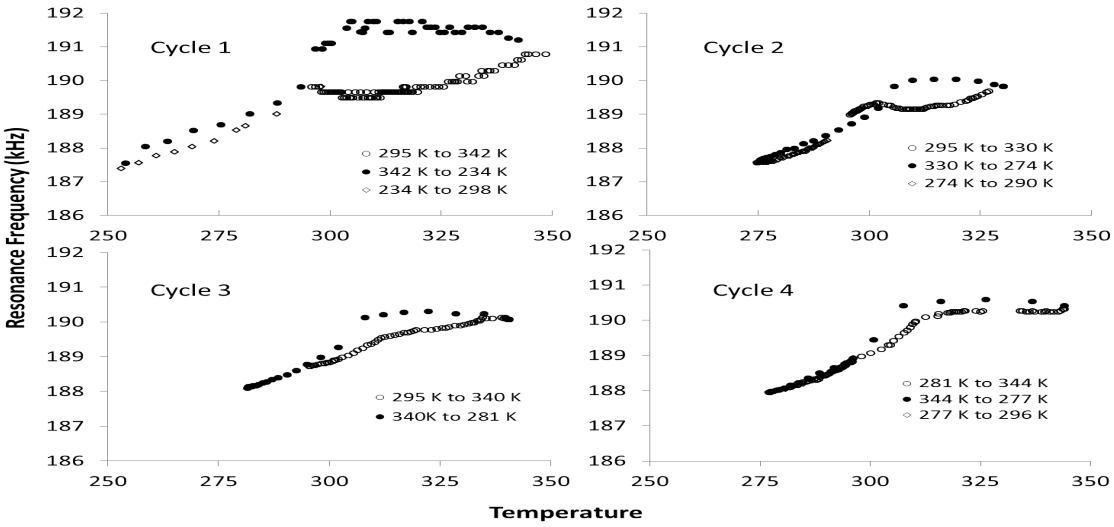

Figure 5.13: Run 2, 7th resonance frequency as a function of temperature. The cycle is labeled in each figure.

Importantly, the sample re-set did not change either the slope of frequency vs temperature or the hysteresis at high temperature seen in Figure 5.12. The hysteretic signature begins between 280 K and 300 K and continues to the maximum temperature that could be imposed on the system, approximately 345 K. Unfortunately, the experimental system was designed to explore temperatures at and below 300 K, and the the solder used on the sample chamber transducers has a melting temperature of 350 K. In magnetic and resistivity studies of ytterbium [19, 22, 23], hysteretic behavior spanned the range 150 K - 370 K depending on the experiment. In contrast, Rosen's original ultrasonic measurements [18] indicated nothing unusual for temperatures below 300 K. Thus, if the system were redesigned for future experiments, it should be prepared to reach temperatures of at least 400 K to explore the fcc paramagnetic to hcp diamagnetic transition fully.

The hysteresis in Figure 5.13 clearly decreases with each temperature

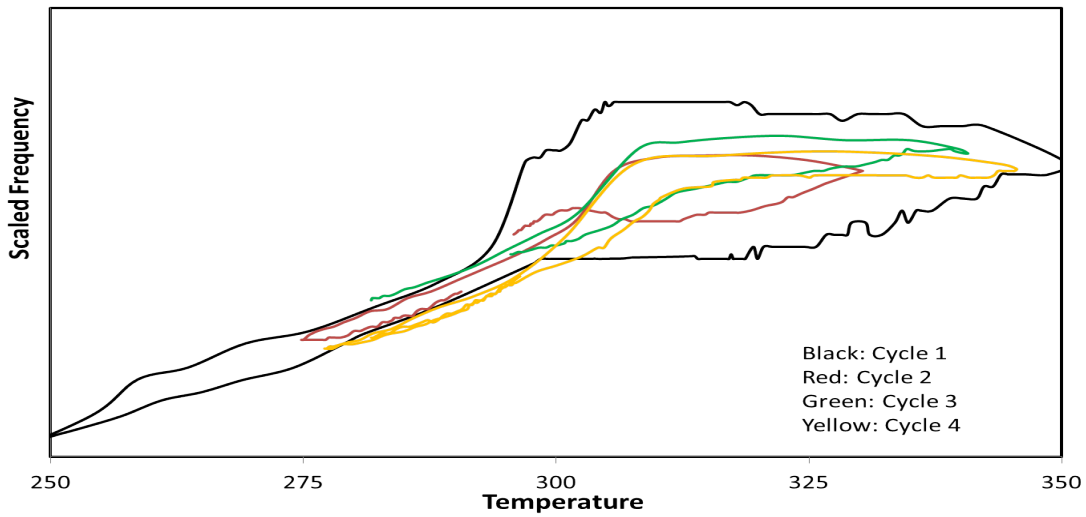

Figure 5.14: Run 2, 7th resonance frequency as a function of temperature. There is a clear trend to decreasing hysteresis. Resonance frequency is scaled in order to make the pattern easier to see.

cycle, until in Cycle 4, there is almost no hysteresis and a transition signature, i.e., a striking change in slope, is apparent at 315 K. This is the temperature at which Bucher [19] reported the magnetic transition from paramagnetic to diamagnetic state on warming. Figure 5.14 shows the trend to decreasing hysteresis with all four cycles overlaid.

5.3.3 Run 3

Run three began at room temperature with liquid nitrogen cooling to 79 K. At this point the data acquisition system failed. Rather then restart an experiment on ytterbium, the sample was removed in favor of a system test using lead. Figure 5.15 shows the temperature response of the sixth and seventh resonance frequencies during the cooling cycle. The data are smooth and otherwise consistent with the previous measurements on the sample.

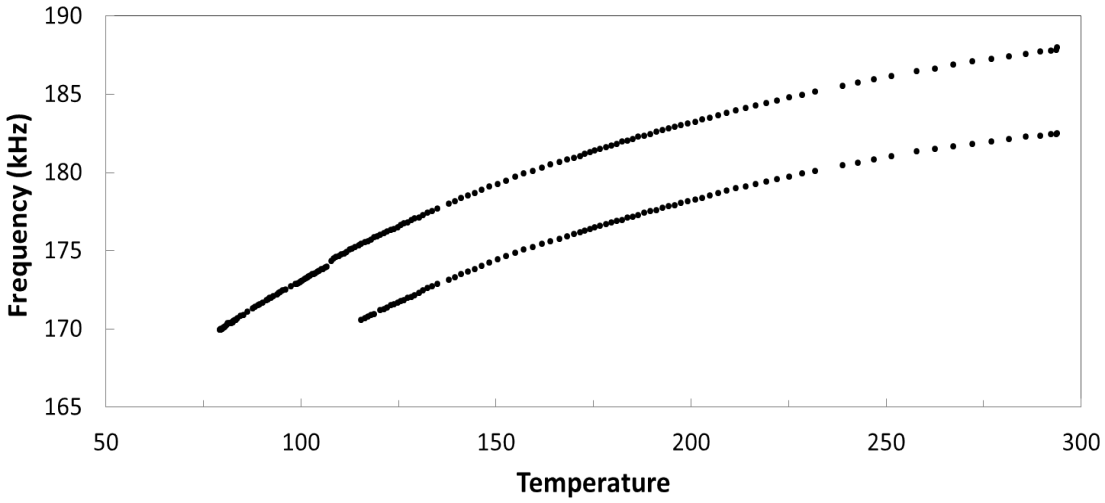

Figure 5.15: Measured sixth and seventh resonances in a cooling cycle on Yb-1. Top curve is the seventh peak, bottom curve is the sixth peak.

5.4 Lead Sample, System Test 1

Between the Yb-1 and Yb-2 experimental runs, a lead sample was used to test the cryogenic system, and temperature control and variation. The Pb sample was cooled from 294 K to 160 K using the liquid nitrogen bath and allowed to warm through diffusive processes; RUS spectra were obtained throughout the cycle. The evolution of the sixth resonance is shown in Figure 5.16, where the peak frequency is plotted versus temperature. Between 160 K and 294 K the behavior is completely linear as expected; there are no indications of phase transitions or hysteresis within the peak-picking accuracy.

Forward calculations of the lead sample's resonances, as described in Section 3.2, indicate that the resonance tracked in Figure 5.16 has a 99% dependence on c_{44}. Thus the resonance is almost pure shear, and the behavior of the resonance frequency squared can be compared to measurements of the shear

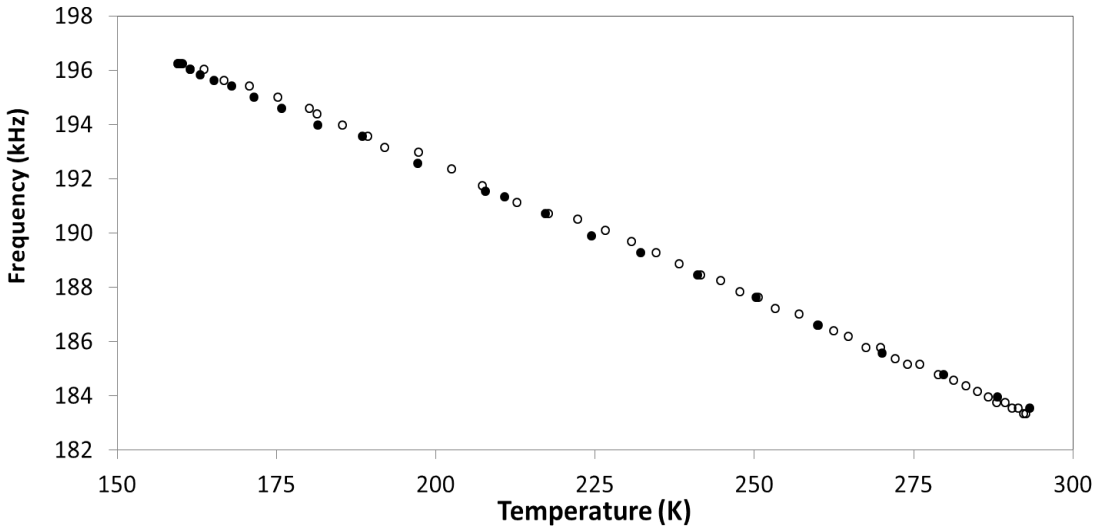

Figure 5.16: A resonance peak frequency of the Pb sample as a function of temperature. Filled circles are resonances during cooling; open circles are resonances during warming.

modulus (see Section 3.4). The normalized resonance frequency squared of this shear-dependent resonance is shown in Figure 5.17 as a function of temperature. The shear modulus, as measured by Waldorf and Alers[35] using an ultrasonic pulse-echo technique, is also plotted on the same scale. In both cases, the change between 300 K and 160 K is almost 15%. The agreement between the two measurements provides confidence that the cryostat and associated experimental apparatus are functioning as designed.

Figure 5.18 shows the temperature profile for the first cycle of the lead experiment. As might be expected, cooling and warming rates are not uniform or symmetric. The cooling rate is dependent on the human-controlled rate of liquid nitrogen addition to the cryostat bath, as well as the heat diffusion rate of the system. Warming is entirely dependent on the heat diffusion rate of the system. Except in cases of active heating, i.e., the heating coils were engaged, every cooling

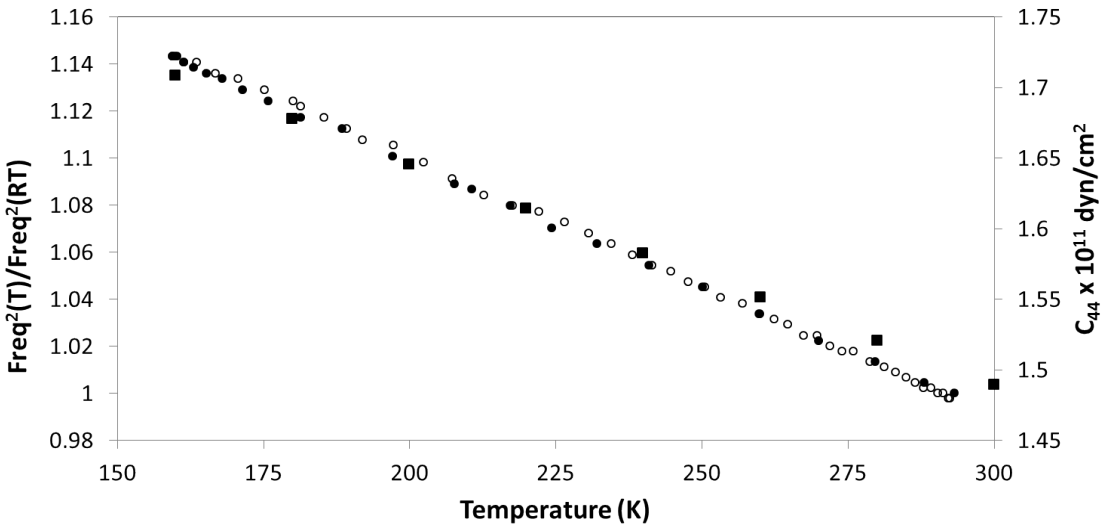

Figure 5.17: Temperature dependence of lead elasticity. The circles are the normalized resonance frequency squared for a shear mode of the lead sample (filled circles are cooling; open circles are warming). The squares are measurements of the shear modulus of lead by Waldorf and Alers[35].

cycle in this dissertation has a similar temperature profile.

5.5 Yb-2 Sample, Run 1

Having gained confidence in the experimental system from the results of measurements on lead, the second ytterbium sample (Yb-2) was chosen for the next set of measurements. The sample was cooled over five hours to 85 K using the liquid nitrogen bath, and 160 RUS spectra were obtained between 120 and 250 kHz. Then, during warming the data acquisition system once again failed, leaving no data record for warming. Nevertheless, the frequency spectra obtained on cooling were clear and consistent, allowing for a reliable inversion for the shear modulus as a function of temperature.

Table 5.9 shows the first eight Yb-2 measured and calculated resonance

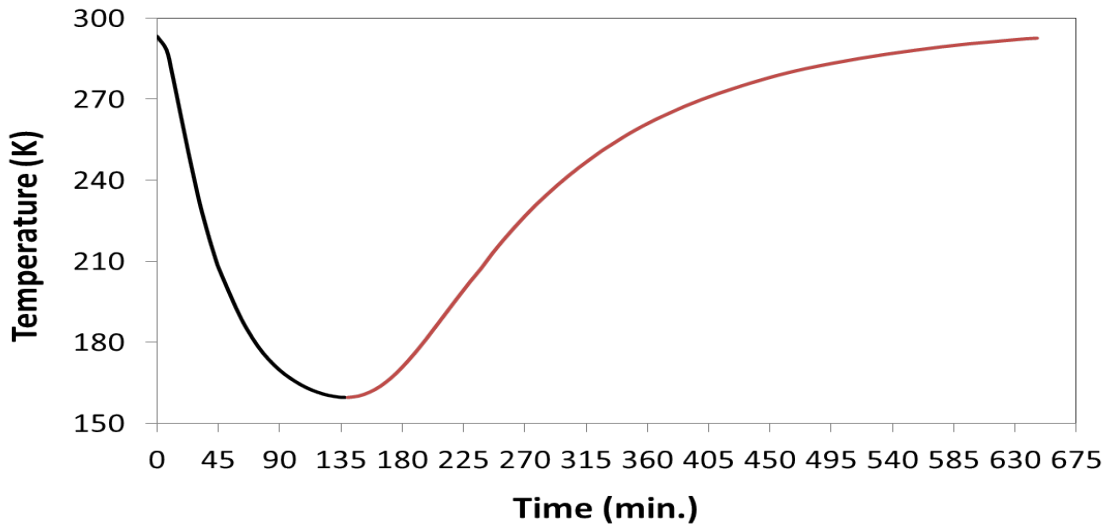

Figure 5.18: Temperature profile for the Pb experiment. Blue curve is cooling, red curve is warming.

frequencies at room temperature and their dependence on the moduli c_{11} and c_{44}. Figure 5.19 shows the evolution of the fourth and fifth resonances, which decrease 8% over 200K. These data from Yb-2 are consistent with the data from Yb-1 shown in Figure 5.15, confirming the unusual positive frequency versus temperature slope. An inversion using the first to eighth resonances gives the c_{44} values shown in Figure 5.20. Also plotted on the figure are normalized frequency squared for the fourth resonance.

5.6 Yb-1 Sample, Run 4

At this point in the sequence of experimental runs, a primary interest was to explore low temperatures to look for a transition from positive to negative slope in resonance frequency versus temperature. However, the original design for temperature control in a large cryostat was turning out to be prohibitively difficult

Resonance	**Frequency (kHz)**	**Calculated (kHz)**	% c_{11}	% c_{44}
1	91.6	91.4	0	100
2	110.6	110.3	22	78
3	113.9	114.3	22	78
4	154.9	154.7	16	84
5	156.5	157.8	4	96
6	163.0	164.3	5	95
7	169.9	169.1	5	100
8	177.3	177.7	4	96

Table 5.9: Measured and predicted 1st - 8th resonance frequencies of Yb-2 at $T = 297$ K. For each resonance, the involvement of the elastic constants, c_{11} and c_{44}, in the resonance is shown.

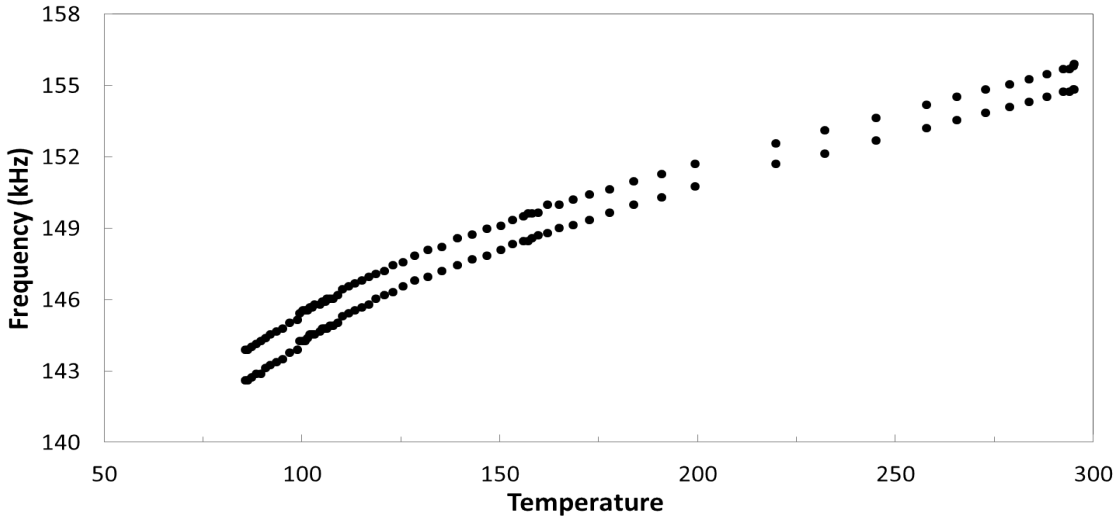

Figure 5.19: Evolution of the fourth and fifth resonance frequencies of Yb-2 Run 1 as a function of the temperature.

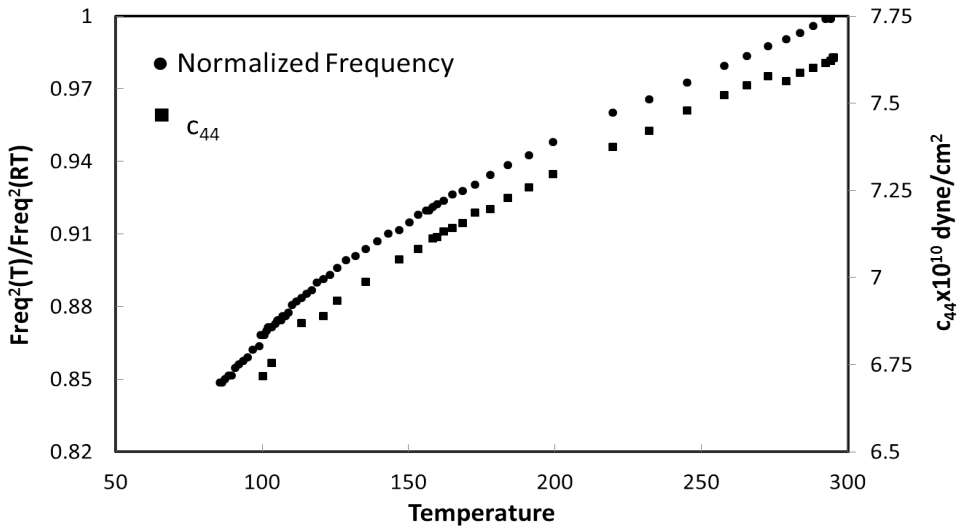

Figure 5.20: The shear modulus of Yb-2, inverted from first to eighth resonances, and the normalized frequency squared of the fourth resonance as a function of temperature. Both change by almost 12% over 200 K.

and expensive to use, since it relies on human control of the addition of liquid helium to a bath for cooling and the evaporation of the liquid helium for warming. Given the high cost of liquid helium and the difficulty maintaining control of temperature, it was reasonable to look for a different cooling method.

At the time, Dr. Timothy Darling, Research Professor at the University of Nevada, Reno, had begun design and construction of an experimental chamber connected to a closed cycle helium refrigerator. The new experimental chamber is slightly smaller but similar to that shown in Figure 4.7. The closed cycle helium refrigerator system has the ability to lower and maintain temperatures to 13 K. Dr. Darling graciously agreed to the use of this system for the remaining experiments that are described in this chapter. Thus, after a seven-month break in experiments, a fourth run of resonance measurements was made on the Yb-1 sample.

Table 5.10 shows the temperature extremes for four almost identical

Date	Run	Cycle	Trend	Initial T (K)	Final T (K)
Nov/Dec 2012	4	First	Cooling	294	13
			Warming	13	293
		Second	Cooling	294	13
			Warming	13	230
		Third	Cooling	294	14
			Warming	14	296
		Fourth	Cooling	296	14
			Warming	14	276

Table 5.10: Temperature extremes during experimental runs on the Yb-1 sample.

temperature cycles. Cooling took approximately three hours and forty five minutes each time, and resulted in approximately 95 RUS spectra. After active cooling, the sample returned to room temperature through diffusive processes rather than active heating. This took approximately 25 hours and resulted in approximately 500 RUS spectra. Each RUS spectrum consists of data at 1024 frequencies in the range 150-192 kHz. This frequency range covers the third to seventh resonances of Yb-1, as shown in Table 5.8.

Figure 5.21 shows the evolution of the seventh resonance over the four cycles of Run 4. There were technical difficulties during the second cycle and much of the warming data was lost. However, data from cycles 1, 3, and 4 cover the entire range of time and temperature. The resonance frequency behavior is consistent over the four cycles, although highly unusual. First, the resonance frequency continues to decrease with decreasing temperature, implying the sample is softening to very low temperature. Second, the low temperature frequency behavior is highly hysteretic; the resonance frequency is higher on cooling than on warming. During cooling, the frequency decreases smoothly, except for a slight knee at 50 K and a subsequent dive

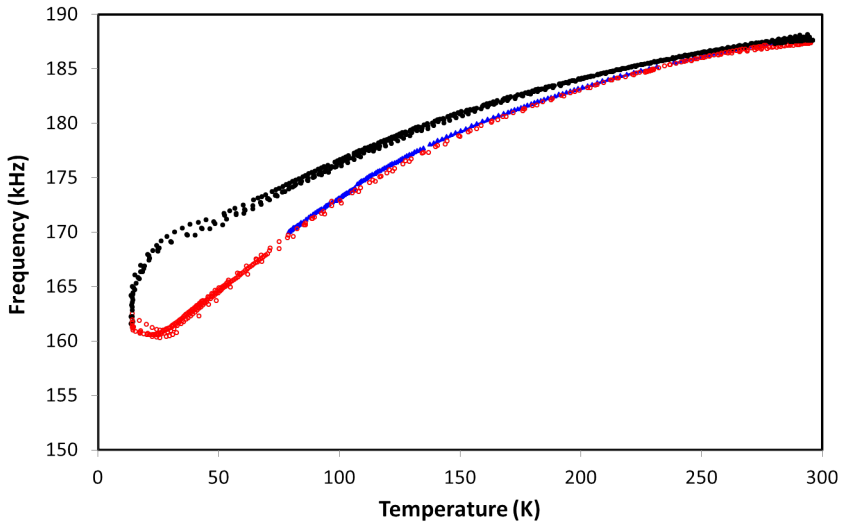

Figure 5.21: Evolution of the seventh resonance frequency of Yb-1 as a function of the temperature during Run 4. Black symbols indicate cooling; red symbols indicate warming. The blue symbols are the 7th frequency data from Figure 5.16 (Run 3).

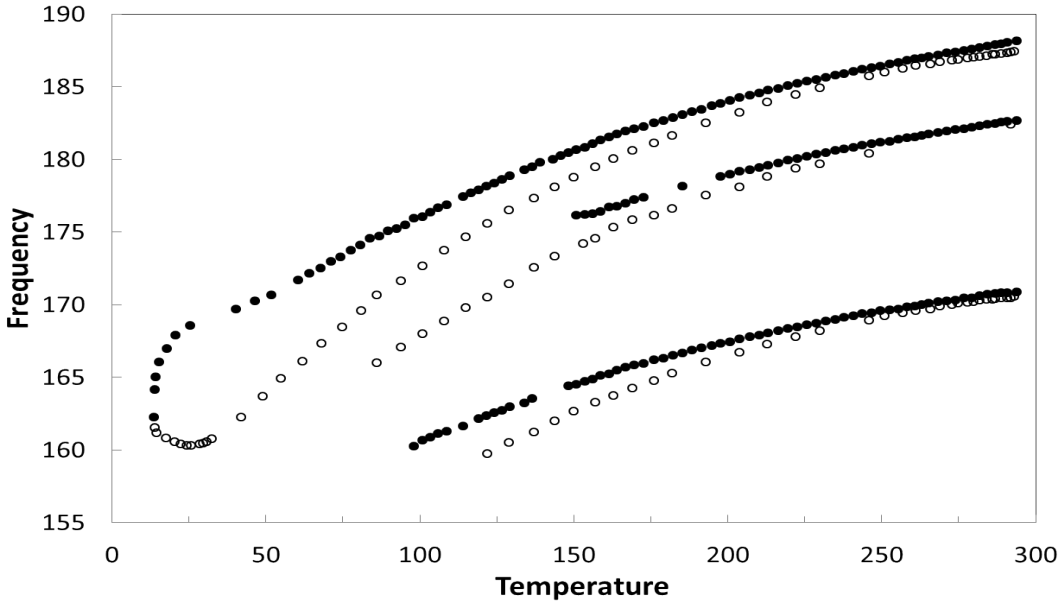

Figure 5.22: Fifth, sixth, and seventh resonances of Yb-1 as a function of temperature for the first cycle of Run 4. Solid symbols indicate cooling, open symbols indicate warming.

in frequency to the lowest temperature achieved in this experiment. Additionally, the initial warming (14 - 25 K) induces a further decrease in the resonance frequency before the frequency begins its return to the initial room temperature value.

The high temperature hysteresis seen in previous measurements is not evident in these data, perhaps because the temperature maximum is below 300 K, and perhaps due to the previous cycling that appeared to be reducing phase disparities in the sample. Other resonances of the Yb-1 sample show a similar trend in frequency versus temperature, although most are difficult to pick at temperatures below 150 K. Figure 5.22 shows the evolution of fifth, sixth, and seventh resonance frequency during the first cycle. The other peaks confirm the lack of high temperature hysteresis, and hint at the presence of low temperature hysteresis.

5.7 Lead Sample, System Test 2

Before moving to measurements on Yb-2, measurements were made on the lead sample again to test for reproducibility of results. During the second system test, the sample temperature was lowered from 294 K to 16 K and allowed to diffusively warm to 128 K. RUS spectra were obtained throughout the temperature cycle over a frequency range of 140 - 350 kHz. Figure 5.23 shows the sixth resonance frequency as a function of temperature for System Test 1 and System Test 2. The data are consistent. The agreement between cooling and warming resonance frequencies indicates that the sample thermally equilibrates more rapidly than the system changes temperature.

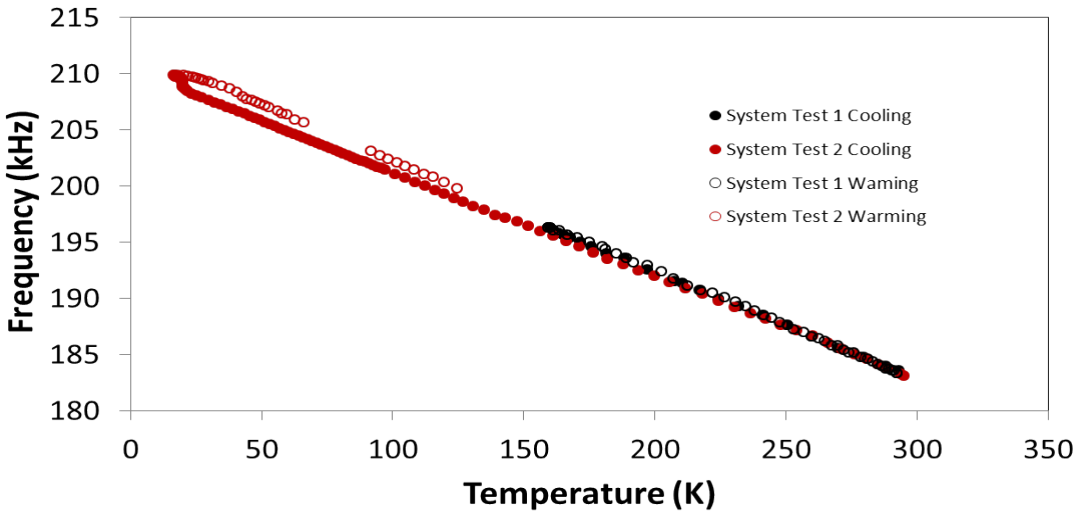

Figure 5.23: Resonance frequency as a function of temperature for System Test 1 and System Test 2.

The sixth resonance is strong and behaves as expected, as shown in Figure 5.24, where the resonance peak is plotted as a function of frequency for several temperatures. At the far left, the room temperature resonance frequency peak is centered at 183.2 kHz. At 16 K, the resonance frequency peak is narrower and has shifted to 209.9 kHz on the far right of the figure. Both the shift to higher frequency and to a narrower resonance peak indicate that the sample becomes harder at lower temperature.

5.8 Yb-2 Sample, Runs 2 and 3

The final set of measurements were performed on the Yb-2 sample using the closed cycle helium refrigerator. Spectra were collected at 1024 frequencies in the range 130-160 kHz. The temperature extremes for Runs 2 and 3 are shown in Table 5.11. Run 2 was essentially a repeat of Yb-1 Run 4, to confirm the hysteretic and other

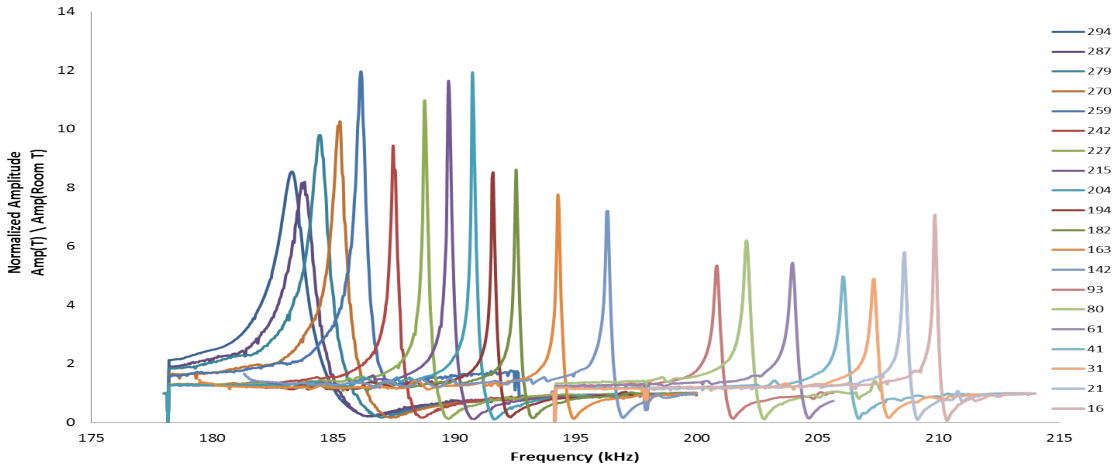

Figure 5.24: A normalized resonance peak of the lead sample as the temperature is lowered from 294 K to 16 K. The peak shifts to higher frequency as the temperature decreases.

interesting behavior. Figure 5.25 shows the evolution of the fourth resonance for three temperature cycles during Run 2. A continuing instability in the data acquisition system caused the loss of some of the warming data in the first two cycles. Nevertheless, the measurements are repeatable and show a similar evolution as the seventh resonance of Yb-1. The resonance frequency decreases with decreasing temperature, is highly hysteretic at low temperature, displays a knee at approximately 50 K, and initially decreases on warming. Interestingly, the knee on cooling and change in slope on warming occur at approximately the same temperature.

In Yb-2 Run 3, the intent was to explore the robustness of the low temperature hysteresis through interior temperature variation. For the purposes of the following discussion, the upper (decreasing temperature) part of the resonance frequency hysteresis loop shown in Figure 5.25 will be called the upper backbone.

Date	Run	Cycle	Trend	Initial T (K)	Final T (K)
December 2012	2	First	Cooling	294	13
			Warming	13	256
		Second	Cooling	294	13
			Warming	13	246
		Third	Cooling	294	13
			Warming	13	294
January 2013	3	First	Cooling	296	15
			Warming	15	95
			Cooling	95	55
			Warming	55	271
		Second	Cooling	295	48
			Warming	48	100
			Cooling	100	38
			Warming	38	169

Table 5.11: Temperature extremes during experimental Runs 2 and 3 on the Yb-2 sample.

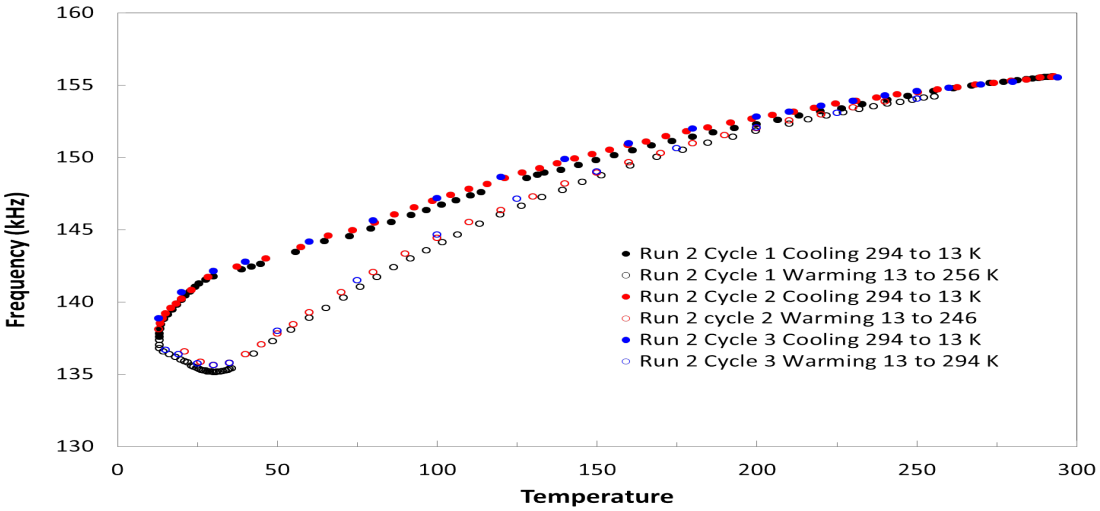

Figure 5.25: Evolution of the fourth resonance for three temperature cycles during Yb-2 Run 2.

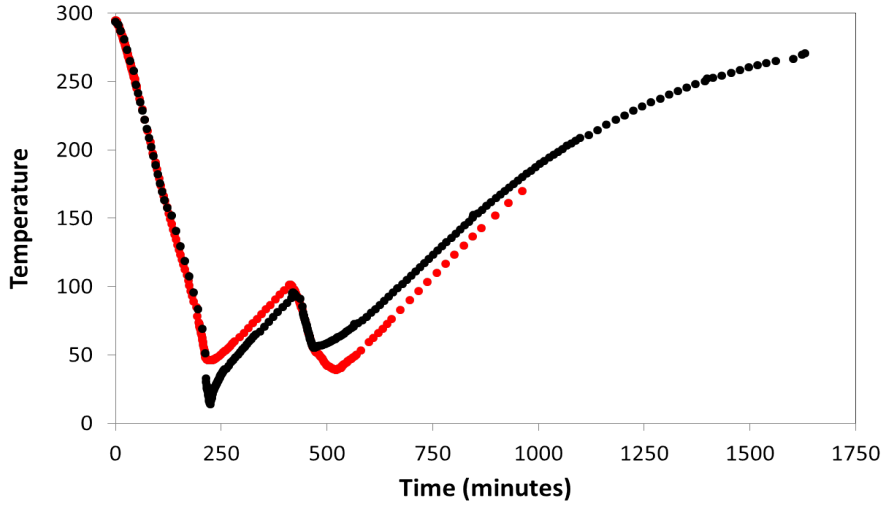

Figure 5.26: Temperature profile as a function of time for Yb-2 Run 3.

The increasing temperature part of the resonance frequency hysteresis loop in Figure 5.25 will be called the lower backbone.

The temperature profiles for the two cycles of Yb-2 Run 3 as a function of time are shown in Figure 5.26. The fourth resonance frequency as a function of temperature is shown for both Run 3 cycles in Figure 5.27, along with the first cycle of Run 2. In the first cycle, the temperature was reduced to 15 K and then increased to 95 K. The resonance frequency behavior up to this point tracks that of the Run 2 cycles, following the upper backbone until the temperature change reverses direction, then diving to meet the lower backbone. At 95 K, the temperature change reversed direction and the temperature was lowered to 55 K. In response, the resonance frequency cuts into the interior of the hysteresis loop, looking as though it could eventually join the upper backbone of hysteresis loop. Before that occurs, the temperature changed direction and the resonance frequency takes a dive to meet up with the lower backbone of the original hysteresis loop.

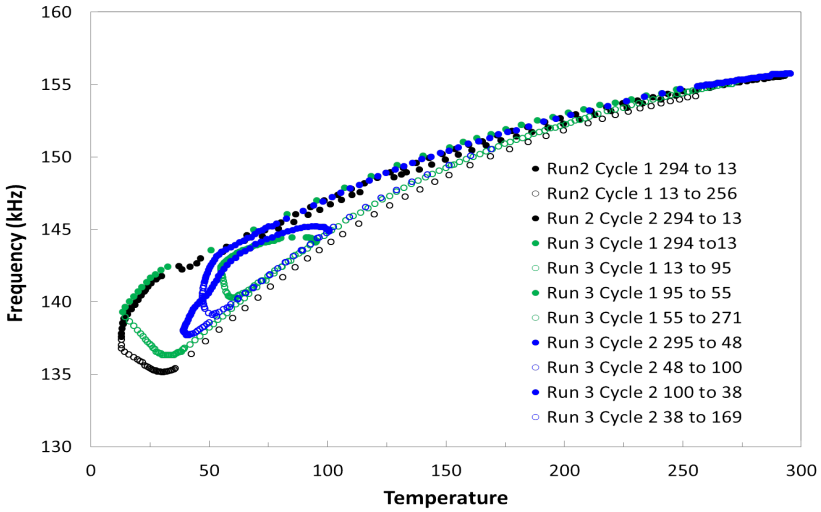

Figure 5.27: Evolution of the fourth resonance frequency of Yb-2 in the first run as a function of the temperature. Each color represents a unique cycle.

With further increase in temperature, the resonance frequency repeats the Run 2 cycle increase, following the lower backbone.

The first cycle of Run 3 seems to imply that the sample resonance response has a well-defined upper and lower hysteresis backbone and that resonance frequency in this temperature regime could be described by models of hysteretic elastic systems with discrete memory [37]. The second cycle of Run 3 make this conclusion less clear. In the second cycle, the resonance frequency departs from the upper backbone before the temperature change reverses direction. Throughout the temperature protocol, the lower backbone of the hysteresis loop remains stable, but the upper backbone seems to have degraded below approximately 60 K. Regretfully, this was the last measurement performed for the purposes of this dissertation. Further confirmation and exploration of the unusual and interesting behavior seen here in ytterbium awaits another researcher.

Chapter 6

Discussion and Conclusion

The techniques and methodology used here are the first of their kind for gadolinium and ytterbium. The gadolinium measurements give results consistent with those previously reported in literature. The ytterbium measurements reveal three unexpected phenomena: a positive slope in resonance frequency versus temperature, high temperature hysteresis that decreases with temperature cycling, and hysteresis at low temperatures with discrete memory characteristics. The following conclusions have been drawn.

1. The results obtained from gadolinium prove the applicability of the extended version of RUS at low temperatures, and show that the system created from scratch performs comparably to a commercial RUS system. The observed behavior of the gadolinium sample was consistent with previous measurements using other techniques. The resonance peaks tracked on the Gd sample were repeatable, had an overall negative slope indicating hardening as temperature decreased, and

showed slope discontinuities around expected transition temperatures. Transitions were observed at approximately 116 K, 222 K and 289 K. The relative change and absolute values of moduli and compressibility compare favorably with those reported in literature [6].

2. Of the unexpected ytterbium results, the high temperature hysteresis is the least surprising. While not observed in pulse-echo measurements, hysteretic behavior has been observed in resistivity, Hall coefficient, and magnetic susceptibility measurements in the temperature range 150 370 K [19, 22, 23], along with evidence for a transition from hcp (diamagnetic) to fcc (paramagnetic) at 315 K. In this work, high temperature hysteresis begins between 280 K and 300 K and continues to 345 K, the highest achievable temperature for this system due to the solder melting temperature. Over consecutive cycles, the hysteresis decreases to reveal a transition signature at 315 K, consistent with the previously reported transition. A future project to explore this hysteresis and transition would involve the development of an experimental system that can perform up to 400 K.

3. The positive slope in resonance frequency versus temperature in ytterbium indicates sample softening as temperature decreases, counter to expectation. This behavior is consistent in this work across samples, runs, and cycles, in two temperature control environments, and over a period of more than a year. Softening is typically observed approaching a phase transition, but it is very extended in these Yb results. Lanthanides owe much of their unusual behavior to the fact that the 4f outer shell electrons are very close in energy to the 6s and 5d

shells. Thus, the character of the electronic bands is sensitive to quite small environmental changes. The softening behavior in Yb could be due to a microstructure/strain defect that isn't observed in pulse-echo measurements. The free boundary conditions preferred for RUS measurements release strain and could allow the observation of behavior that is inhibited by pulse-echo measurements, where transducers are physically bonded to faces of the sample, inducing strain rather than releasing it. A future project to explore the hypothesis of a strain defect would involve neutron diffraction experiment, to learn more about the strain in the lattice planes of the material grains.

4. The softening observed in Yb suggests a structural phase transition at a temperature below 20 K. No such transition has been reported for this material, so exploration of extremely low temperatures would also fall on the future projects list. This softening may be related to the long softening seen in low temperature martensitic transformations. Similar behavior has been observed in alloys of polycrystalline gold-zinc (AuZn), which have other behavioral similarities to lanthanides. AuZn softens to a martensitic transformation near 64 K and then resume normal behavior (hardening) to 4K [38]. In this work, it appears that the transition in Yb has not been reached.

5. The low temperature hysteresis displayed by Yb was repeatable and did not decrease in magnitude, as for the magnetic transition at 315 K. In fact, there is some indication that the low temperature hysteresis shows discrete memory [37] and is thus a fundamental characteristic of the material. Future work should definitely

plan on exploring this hypothesis with carefully planned temperature cycles at very low temperature. Hysteresis is generally associated with a first-order phase transition in which an energy barrier must be crossed. However, at low temperatures, i.e., low energies, first-order transitions tend to be suppressed. The very close energies of the 4f, 6s, and 5d electrons in Yb may allow the material to be sensitive to otherwise suppressed transitions.

6. Additional material characterization might reveal more about the unusual behavior observed in the Yb samples. Limited studies of the samples under a microscope were performed to search for cracks, holes, voids or bubbles. None were observed. In addition, the calculated densities of the samples based on mass and dimensions match the generally accepted density, indicating that the samples are reasonably homogeneous. Further studies using x-ray diffraction to learn more about the sample crystal structure, or neutron scattering to probe magnetic transitions, would be useful. A single crystal RUS measurement would be an outstanding way to obtain additional information, however, the production and aligning of single crystals is quite difficult.

7. The data acquisition technique used in this work should be improved for future measurements with long experimental run times. Data loss could be minimized by using more secure and sophisticated methods of storing, handling, and interpreting data.

Although experiencing the unexpected is one the greatest joys in science, it can also be one of the greatest frustrations. The research and observations described

here are the result of several years of planning, building and testing, and yet ended without a conclusive result. Perhaps its value lies in descriptions of what worked experimentally and what did not in the application of resonant ultrasound spectroscopy to lanthanides, and in tweaking the curiosity of the next researcher to explore the behavior of polycrystalline ytterbium.

Bibliography

[1] "DOE Fundamentals Handbook:Nuclear Physics and Reactor Theory," *U.S. Department of Energy*, January 1993.

[2] J. B. Hedrick, "Rare Earths in Selected U.S. Defense Applications," 40^{th} Forum on the Geology of Industrial Minerals, 2004.

[3] C. K. Gupta and N. Krishnamurthy, "Extractive Metallurgy of Rare Earths," CRC Press, p. 32, 2004.

[4] http://www.everyscience.com/Chemistry/

[5] D. A. Young, "Phase diagrams of the elements," University of California Press, pp. 207 - 212, 1991.

[6] M. Rosen, "Elastic Moduli and Ultrasonic Attenuation of Gadolinium, Terbium Dysprosium, Holmium, and Erbium from 4.2 to 300 °K," *Phys. Rev.*, 174, p. 504, 1968.

[7] C. Kittel, "Introduction to Solid State Physics," Wiley, 1996.

[8] D. C. Jiles and S. B. Palmer, "Magnetoelastic effects in gadolinium," *J. Phys. F: Metal Phys.*, 10, pp. 2857-2866, 1980.

[9] V. Yu. Bodriakov, A. A. Povzner, and S. A. Nikitin, "Magneto-phonon contribution into the Young's modulus of gadolinium," *Eur. Phys. J. B*, 4, pp. 441-445, 1998.

[10] Y. I. Spichkin, A. M. Tishin, and K. A. Gschneidner Jr., "Elastic propoerties of a high purity gadolinium single crystal," *J. Magn. Magn. Mater.*, 204, pp. 5-10, 1999.

[11] C. D. Graham, "Magnetocrystalline Anisotropy of Gadolinium," *J. Phys. Soc. Jpn.*, 17, pp. 1310-1310, 1962.

[12] R. M. White and T. H. Geballe, "Long Range Order in Solids," Academic Press, 1979.

[13] K. A. Gschneidner, Jr. and Le Roy Eyring, "Handbook on the Physics and Chemistry of Rare Earths, Chapter 6 Magnetic and Transport Properties of the Rare Earths," Vol 1, chapter 6, p. 431.

[14] J. W. Cable and E. O. Wollan, "Neutron Diffraction Study of the Magnetic Behavior of Gadolinium," *Phys. Rev.*, 165, p. 166, 1968.

[15] W. D. Corner and B. K. Tanner, "The Easy Direction of Magnetization in Gadolinium," *J. Phys. C: Solid State*, Vol. 9, p. 627, 1976.

[16] J. F. Smith, C. E. Carlson, and F. H. Spedding, *J. Metals*, 9, 1212, 1957.

[17] W. H. Gust and E. B. Royce, "New Electronic Interactions in Rare-Earth Metals at High Pressure," *Physical Review*, B8, 1973.

[18] M. Rosen, "Elastic Moduli of Thulium and Ytterbium From 4.2 to 300°K," *Journal of Physics and Chemistry of Solids*, Volume 32, Issue 10, 1971

[19] E. Bucher, P. H. Schmidt, A. Jayaraman, K. Andes, J. P. Maita, K. Nassau, and P. D. Dernier "New First-Order Phase Transition in High-Purity Ytterbium Metal," *Physial Review B 2*, 1970.

[20] M. Rieux, "Phase Hexagonale De L'ytterbium Sous Pression," *Solid State Communications*, Vol. 9, pp 1179-1181

[21] S. Tanuma, W. R. Datars, H. Doi and A. Dunsworth, "The de Haas-van Alphen Effect in HCP Ytterbium," *Solid State Communications* Vol 8, Issue 8, p 1107-1110.

[22] J. E. A. Alderson and C. M. Hurd, "Hall Effect Studies in Ytterbium Through The fcc-hcp Transformation," *Solid State Communications* Vol. 11, p. 1245-1248, 1972.

[23] F. X. Kayser, "Polymorphic Transformation in Ytterbium," *Physical Review Letters* Vol 25, Number 10, p. 662, 1970.

[24] J. Maynard, "Resonant Ultrasound Spectroscopy," *Physics Today*, Volume 49(1), pp. 26-31, Jan 1996.

[25] A. Migliori and J. L. Sarrao, "Resonant Ultrasound Spectroscopy," Wiley-Interscience, 1997

[26] R. B. Schwarz, and J. F. Vuorinen, "Resonant Ultrasound Spectroscopy: Applications, Current Status and Limitations," *Journal of Alloys and Compounds*, 310, pp. 243-250, 2000.

[27] D. B. Frazer, and R. C. LeCraw, "Novel Methods of Measuring Elastic and Anelastic Properties of Solids," *Rev. Sci. Instrum.*, Volume 35, page 1113, 1964.

[28] N. Soga, and O. L. Anderson, "Elastic Properties of Tektites Measured by Resonant Sphere Technique", *Journal of Geophysical Research*, Volume 72(6), p. 1733, 1967.

[29] H. H. Demarest Jr., "Cube Resonance Method to Determine the Elastic Constants of Solids", *J. Acoust. Soc. Am.*, Volume 49(3B), pp. 768-775, 1971.

[30] I. Ohno, "Free Vibration of a Rectangular Parallelepiped Crystal and Its Application to Determination of Elastic Constants of Orthorhombic Crystal", *Journal of Physics of the Earth*, Volume 24(4), pp. 355-379, 1976.

[31] W. M. Visscher, A. Migliori, T. Bell, and R. A. Reinert, "On the normal modes of free vibration of inhomogeneous and anisotropic elastic objects," *Journal of Acoustical Society of America*, 90 (4), Pt. 1, October 1991

[32] A. Fetter, and J. D. Walecka, "Theoretical Mechanics of Particles and Continua", Dover, 2003

[33] D. W. Marquardt, "An Algorithm for Least-Squares Estimation of Nonlinear Parameters", *Journal of the Society for Industrial and Applied Mathematics*, 11 (2), p. 431, 1963.

[34] W. H. Press, B. P. Flannery, S. A. Teukolsky, and W. T. Vetterling, "Numerical Recipes," Cambridge, 1986

[35] D. L. Waldorf and G. A. Alers, "Low-Temperature Elastic Moduli of Lead", *Journal of Applied Physics*, 33, p. 3266, 1962.

[36] Varshni, A., "Temperature dependence of the elastic constants", *Phys. Rev.* B, 40, 341-354, 1974.

[37] K. R. McCall and R. A. Guyer, "Equation of state and wave propagation in hysteretic nonlinear elastic materials", *J. Geophys. Res.*, 99, p. 23,887, 1994.

[38] https://arxiv.org/ftp/cond-mat/papers/0108/0108168.pdf